Composites Part B

Design, novel quality check and experimental test of an original variable length stepped scarf repair scheme

--Manuscript Draft--

Manuscript Number:	
Article Type:	Full Length Article
Keywords:	Composite repair; stepped scarf joint; finite element analysis
Corresponding Author:	Mahdi Damghani University of The West England (UWE) Bristol, North somerset United Kingdom
First Author:	Mahdi Damghani, PhD
Order of Authors:	Mahdi Damghani, PhD
	Stephan Bolanos, BEng
	Amandeep Chahar, BEng
	Gary A. Atkinson, PhD
	Jason Matthews, PhD
	Adrian Murphy, PhD
	Timothy Edwards, MSc
Manuscript Region of Origin:	Europe
Abstract:	Previous works have studied the performance of well-established stepped scarf repair schemes for highly loaded composite structures. However, none of the proposed repair schemes appear to minimise healthy material removal. Thus, this paper, proposes a Variable Length Stepped Scarf (VLSS) scheme, which minimises healthy material removal. In addition, various standard schemes with overlap step length (1/60, 1/45 and 1/30) are studied. Both experimental and simulation (FEA) investigations are undertaken and for the first time, the quality of scarf is inspected by artificial-intelligence based machine vision. The experimental results show the VLSS scheme is comparable to the other repair designs in restoring structural stiffness of the intact structure. The VLSS shows the ability to restore 95% stiffness of the pristine structure compared to 91.4% of the largest repair scheme (overlap step length = 1/60). However, the VLSS scheme falls short in restoring the static strength of the structure, with an efficiency of 64%. By contrast, the largest repair scheme shows a superior strength repair efficiency 77% and demonstrates a desirable failure response, i.e. fibre fracture in both repair patch and parent laminate.
Suggested Reviewers:	Carol Featherston, PhD Research theme leader, Cardiff University featherstonca@cardiff.ac.uk Expert in the field
	Richard Butler, PhD Professor of Mechanical Engineering, University of Bath R.Butler@bath.ac.uk Expert in the field
Opposed Reviewers:	

Dr. Mahdi Damghani

(CEng MIMechE, PhD, MSc, BSc)
Senior Lecturer in Composites and Aero-structures
Room 3D26
Engineering Design and Mathematics Department
University of the West of England (UWE)
Frenchay Campus
Coldharbour Lane
Bristol
BS16 1QY
Tel: 0117 328 7369
Email: Mahdi.Damghani@uwe.ac.uk

Date: 17/08/2021

Dear Editor,

I am pleased to submit an original research article titled “Design, novel quality check and experimental test of an original variable length stepped scarf repair scheme” by Mahdi Damghani[1], Stephan Bolanos[2], Amandeep Chahar[2], Gary A. Atkinson[3], Jason Matthews[4], Adrian Murphy[5], Timothy Edwards[6] for consideration for publication in the *Journal of Composite Part B: Engineering*. This article is prepared by people who are actively involved in the design and analysis of composite aerospace structures having considerable experience with industrial leaders such as Airbus UK and Rolls-Royce. This article focuses on extensive experiments designed by simplified numerical methods using fully characterised and calibrated material model for woven fabric composites. This paper provides a unique perspective to the scientists and engineers on the advantages of the use of size minimisation and hence light weighting when repairing highlight load composite structures yet attempting to maintain structural performance.

This article has not been published and is not under consideration for publication elsewhere.

Thank you for your consideration.

Yours’ Sincerely

Dr. Mahdi Damghani

---

[1] Senior Lecturer of aerostructures at aerospace department of the University of the West of England (UWE), Tel: +4411732 87369, Email: Mahdi.Damghani@uwe.ac.uk
[2] Research students at the aerospace department of the University of the West of England (UWE)
[3] Senior lecturer of machine vision at Bristol Robotic Lab (BRL) of UWE
[4] Senior Lecturer of manufacturing at mechanical engineering department of UWE
[5] Professor of aeronautical engineering at school of mechanical and manufacturing of Queen’s University Belfast (QUB)
[6] Chief engineer and head of engineering at advanced engineering unit of Atkins

- A novel minimum size Variable Length Stepped Scarf (VLSS) and machine vision technique for quality control of scarfed laminates are introduced and performance of VLSS is compared against well-established stepped scarf repair schemes for highly loaded composite structures.
- The VLSS shows the ability to restore $\approx 95\%$ stiffness of the pristine structure compared to 91.4% of the largest repair scheme (overlap step length $\approx 1/60$).
- The VLSS scheme falls short in restoring the static strength of the structure, with an efficiency of 64%.
- The largest repair scheme shows a superior strength repair efficiency $\approx 77\%$ and demonstrates a desirable failure response, i.e. fibre fracture in both repair patch and parent laminate.

Design, novel quality check and experimental test of an original variable length stepped scarf repair scheme

Mahdi Damghani[1], Stephan Bolanos[1], Amandeep Chahar[1], Gary A. Atkinson[1], Jason Matthews[1], Adrian Murphy[2], Timothy Edwards[3]

[1] Department of Engineering, Design and Mathematics (EDM), University of the West of England (UWE), Bristol, BS16 1QY, UK

[2] School of Mechanical and Aerospace Engineering, Queen's University Belfast (QUB), Belfast, BT9 5AG, UK

[3] Advanced Engineering Unit, Atkins, Bristol, BS32 4RZ, UK

Abstract

Previous works have studied the performance of well-established stepped scarf repair schemes for highly loaded composite structures. However, none of the proposed repair schemes appear to minimise healthy material removal. Thus, this paper, proposes a Variable Length Stepped Scarf (VLSS) scheme, which minimises healthy material removal. In addition, various standard schemes with overlap step length ($1/60$, $1/45$ and $1/30$) are studied. Both experimental and simulation (FEA) investigations are undertaken and for the first time, the quality of scarf is inspected by artificial-intelligence based machine vision. The experimental results show the VLSS scheme is comparable to the other repair designs in restoring structural stiffness of the intact structure. The VLSS shows the ability to restore $\approx 95\%$ stiffness of the pristine structure compared to 91.4% of the largest repair scheme (overlap step length $= 1/60$). However, the VLSS scheme falls short in restoring the static strength of the structure, with an efficiency of 64%. By contrast, the largest repair scheme shows a superior strength repair efficiency $\approx 77\%$ and demonstrates a desirable failure response, i.e. fibre fracture in both repair patch and parent laminate.

Keywords: Composite repair, stepped scarf joint, finite element analysis

1 Introduction

In recent years, there has been a significant increase in the use of laminated Carbon Fibre Reinforced Polymer (CFRP) in the design of highly loaded structural components such as aircraft wing primary structures (inc. fuselages, wings, tails, doors, interior, etc) and wind turbine blades [1]. In addition to significant static strength and stiffness, these materials also demonstrate appreciable fatigue performance [2]

and corrosion resistance [3], particularly crucial for high-performance structures with long service life.

Composite aircraft structures will be subjected to accidental damage during manufacture and throughout their life, from tool drop to collision with ground equipment. Significant inflight damage may also take place due to lightning and bird strike [4]. If the damage has weakened the structure through fibre fracture, delamination or debonding, then repair is required. The repair will involve replacement of the damaged fibre reinforcement to restore the original mechanical properties, i.e. stiffness, strength and durability [5]. Such repairs may be achieved via mechanical fastening, adhesive bonding or hybrid fastening and bonding. Generally, bonded repairs to primary (flight-critical) components are desirable, as they do not require mechanical fasteners- resulting in lighter and more aerodynamic repairs. However, such repairs are only permitted when damage after clean-up is not critical at limit/service load [5]. This conservative fail-safe requirement ensures that if the patch bond fails, the structure will have appropriate reserve strength to complete the flight safely [6], [7]. Thus, the need to design joints with a shear dominant stress state with minimum peel in the adhesive layer [8] has resulted in a focusing of the literature on the behaviour and strength performance of stepped or ramped scarf repairs with small scarf angles [8]–[10]. A summary of recent works is presented in Table 1.

Table 1: Summary of repair types and their efficiency in the literature

Researcher	**Repair type**	**Research procedure**	**Scarf angle**	**Loading type**	**Repair efficiency**
Wu et al. [11]	Ramped Scarf & Stepped scarf	Numerical	3^o	Uni-axial tensile	100%-20% depending on flaw size
Liao et al. [12]	Double ramped scarf	Numerical	10^o-33^o	Uni-axial tensile	80%-30%, respectively
Ghazali et al. [13]	Stepped scarf	Numerical & experimental	3^o	Compressive via four-point bending test	≈86%
Han et al. [14]	Stepped scarf	Numerical & experimental	4^o	Uni-axial tensile	N/A
Wang et al. [15]	Stepped scarf	Experimental	3^o	Compressive	≈85% for step length of $20t$*
Psarras et al. [16]	Stepped scarf	Numerical & experimental	1.68^o	Uni-axial tensile	≈69% for step length of $30t$

*t being step height

Resultantly, certified repair schemes are constrained to a narrow set of joint designs, which are typically axisymmetric or plane symmetric for which significant

experimental data and flight experience is available [8], [10], [17]. Although recoverable static strength has been demonstrated between 20%-83% [18], [19] (the latter being for a scarf angle of 2^{o}), the need for small scarf angles is a major weakness: for damage of any significant depth, the repair patch area may be many times larger than the original damage area. Thus, there is a need for a less constrained repair scheme which is optimisable to both local parent laminate and flight loads, such that structural performance may be recovered whilst minimising unflawed material removal. It should be stated that the key advantages of reducing healthy material removal stemming from small repairs are:

- Less intrusion into parent structure, so less likelihood of encountering stiffeners, cut-outs, reinforcements, etc that might complicate the repair scheme;
- Reduced preparation and fabrication time;
- Simpler out-of-autoclave lay-up and curing procedure;
- Reduced inspection time;
- Reduced probability of quality issues in the repair.
- Maintaining aerodynamic cleanliness and minimising disturbance to the structure's original load path, particularly reducing inevitable load eccentricity resulting from the asymmetry of bonded repairs. Such load eccentricities could lead to unwanted failure modes;
- On composite control surfaces (flaps, ailerons etc.) which have critical mass balance limitations, the minimum size hence the lighter weight flush scarf repair is often the only acceptable means of repair [20].

A typical repair process for composite structures is shown in Figure 1. It is worth noting that this figure is collated by the authors based on consultation from leading aerospace companies in the field. Thus, the figure is reflective of current industrial practices.

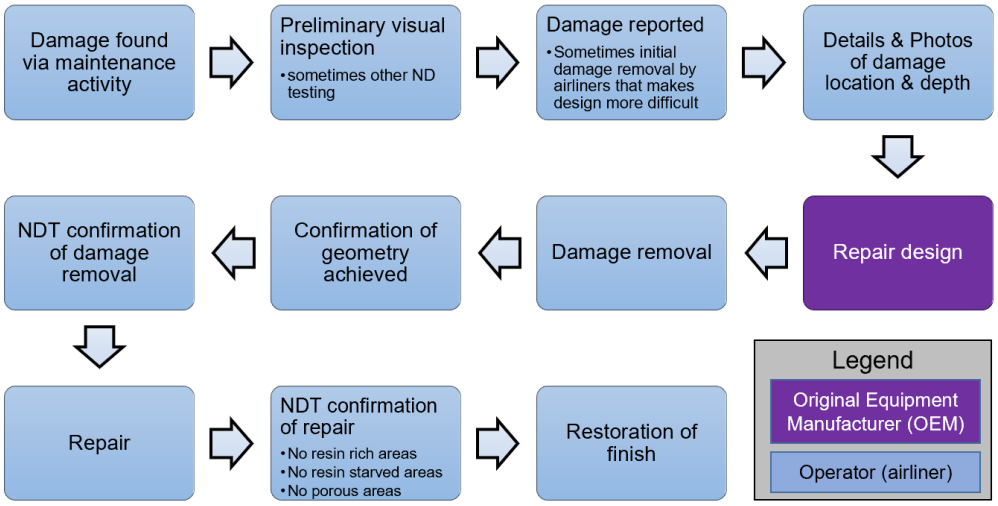

Figure 1: Current laminated composite repair process in industry

This paper investigates the feasibility of a proposed repair scheme known as Variable Length Stepped Scarf (VLSS) repair. The proposed scheme aims to realise a bonded repair of minimum size whilst restoring the required static stiffness and strength of the structure. In addition, a novel inspection/quality assurance process (via machine vision) is proposed and demonstrated. The main novel contribution of this paper is to show that it is possible to minimise healthy material removal while maintaining a structure's stiffness comparable to more established repair methods and suffering only modest reductions in failure loads or displacements.

The remainder of this paper is organised as follows. In section 2 the problem at hand is elaborated and VLSS repair is introduced. The design of stepped scarf repair, preparation of the laminate and inspection of the prepared laminates are discussed in section 3. Results and discussions from simulation predictions and mechanical tests are provided in section 4. Finally, conclusions are made and future works are proposed in section 5.

2 Background

2.1 Problem statement

Typical bonded repairs on aerospace composites require a patch that is joined with scarfed joints to the parent material, as illustrated in Figure 2.

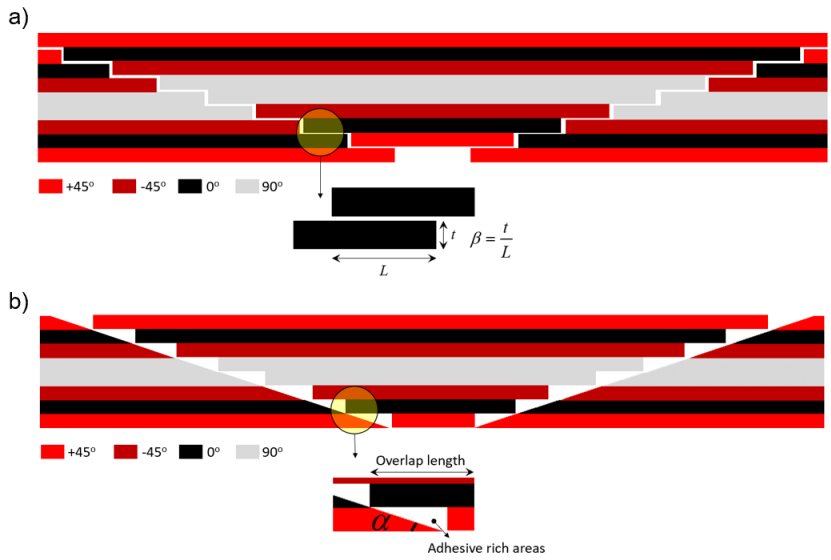

Figure 2: Examples of laminated composite repair schemes, a) stepped scarf repair and b) ramped scarf repair as seen in the literature

Such repairs are currently applied only to aircraft secondary structures and constrained to be near flush with any aerodynamic surface. In the case of a *stepped scarf repair* (see Figure 2a), the current practice requires scarf step parameter ($\beta = t/L$) values of 1/45 (for Boeing) and 1/60 (for Airbus) [21]. These β values lead to prohibitively large repairs and considerable removal of healthy material. In the case of a *ramped scarf repair* (see Figure 2b), it has been shown in [22], [23] that a ramp of $50:1$ is required to achieve maximum strength in the joints, although such ramps achieve slightly less than the full strength of the parent material. The lap length for each repair ply naturally becomes 50 times the ply thickness ($50t$), while the peel load at the attachment of each repair ply is one fiftieth of the in-plane load. Furthermore, the current design methodology for scarf repairs recommends that the scarf angle be determined by analysing a scarf joint representing the most highly loaded section in a three-dimensional scarf repair. Such an idealisation approach is conservative and the beneficial effect of load bypass by the parent structure around the patch is neglected [23].

2.2 Repair application using VLSS joint

The alternative to using a ramped scarf joint of the type illustrated in Figure 2b is the *Variable Length Stepped Scarf repair* as shown in Figure 3, i.e. VLSS. The inevitable discontinuities that exist in the fibres at the repair joint are countered by a series of lap joints that transfer load, through bonds, from fibres in a parent ply to those in an adjacent, overlapping repair ply [11], [14]. It is an axiom of this type of repair that

the material stiffness of the overlapping repair ply should match that of the underlying parent ply in order that load should transfer successfully through the stack of plies (laminate).

The direct force normal to the joint and the shear force acting parallel to the joint in the parent ply determine the total force transferred through each lap joint within the stack. The total force in the ply dictates the required area of the lap, so the areas of the laps will generally be different as different plies carry different loads. For example, if fibres in a uni-directional ply lie tangential to the joint line (the grey ply in Figure 3), little load will be transferred through the lap joint, so the lap length may be short. However, if fibres in a uni-directional ply lie normal to the joint line (the black ply in Figure 3), a longer lap length will be required. Varying the lap lengths in this manner and removing the resin-rich lengths of the ramped scarf joint (Figure 2b), serve to minimise the overall joint length, reducing the size of the repair.

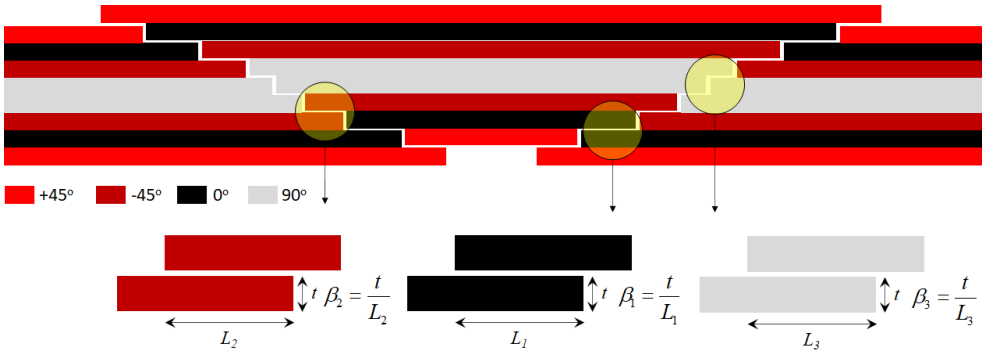

Figure 3: A variable length stepped scarf repair (VLSS)

The integrity of the lap joints that constitute such a repair will be less susceptible to process variation than those of a ramped solution. This is due to the controlled bond thickness (which is not feasible in a ramped solution on account of the resin-rich regions) and the elimination of kinks in the repair plies (which generate peel stresses). It is worth noting that the success of such a repair is heavily reliant on the quality of repair manufacture and the adhesive-adherend bond strength in particular.

Hence, in this paper, the authors study the feasibility and maturity of current technologies (NC milling and finite element analysis) and developing/emerging technology (inspection via machine vision) in implementing the proposed VLSS repair scheme. Furthermore, the VLSS repair scheme will be compared to other existing *stepped scarf repairs*.

3 Methodology

3.1 Materials

The composite material used in this study is twill woven pre-impregnated carbon fibre (AX-5180), with mechanical properties given in the Appendix (Table A1). The carbon prepregs consist of 54% fibre by volume (60% by weight). The adhesive used is XA120 150g film with minimum and maximum cure temperatures of $80^o C$ and $120^o C$, respectively. The mechanical properties for the adhesive have been measured in house and are given in the Appendix (Table A2). The stress-strain curve of the tensile tests for three specimens of the adhesive (Figure A1) exhibit a brittle fracture behaviour.

3.2 Repair designs

Four repair designs A, B, C and D are studied as shown in Figure 4. Each design laminate has dimensions of $280\,mm \times 130\,mm$. In the design A, the scarf step parameter for both the 0^o (β_1) and 45^o (β_2) plies are equal (being $1/30$, i.e. $\beta_1 = \beta_2 = 1/30$). For design B, $\beta_1 = \beta_2 = 1/45$ matching the requirement by some aircraft Original Equipment Manufacturers (OEMs), for example Boeing. Design C represents a more conservative OEM practice, for example Airbus, where $\beta_1 = \beta_2 = 1/60$. Design D is proposed by the authors (see section 3.3) in which the scarf step parameter for the 0^o and 45^o plies are different. In this case, the β values are defined to produce a smaller repair (compared to the previous designs), i.e. $\beta_1 = 1/20$ for $0/90^o$, $\beta_2 = 1/10$ for $\pm 45^o$. As explained earlier, this is because the overlap length for the $\pm 45^o$ plies does not need to be as large as the $0/90^o$ plies owing to a lesser load carrying capability of the $\pm 45^o$ plies (compared to the $0/90^o$ plies). Figure 5 shows the repair plies for all design configurations with the total area of each design normalised to that of Design C. It can be seen that the proposed VLSS scheme, design D, is significantly smaller (39.29%) than the design C.

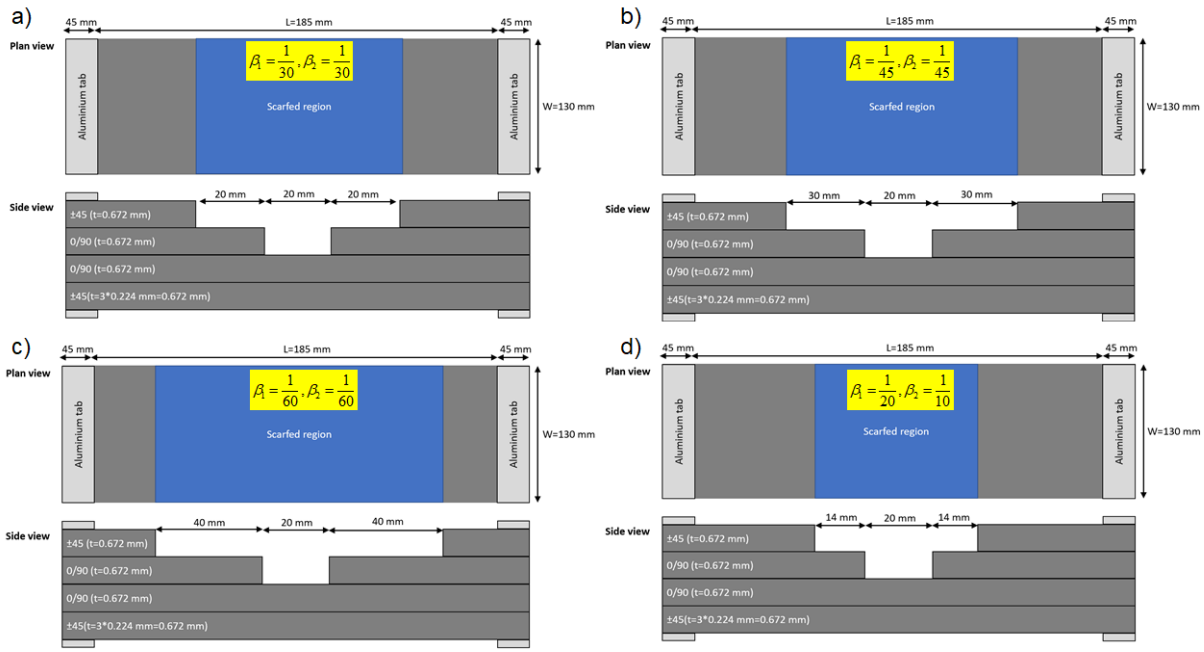

Figure 4: Illustration of repair designs, a) Equal overlap length for $0/90_3^o$ (β_1) and $\pm 45_3^o$ (β_2) plies $\beta_1 = \beta_2 = 1/30$, b) Equal overlap length for $0/90_3^o$ and $\pm 45_3^o$ plies $\beta_1 = \beta_2 = 1/45$, c) Equal overlap length for $0/90_3^o$ and $\pm 45_3^o$plies $\beta_1 = \beta_2 = 1/60$, d) Different overlap length for $0/90_3^o$ and $\pm 45_3^o$plies $\beta_1 = 1/20, \beta_2 = 1/10$ (not drawn to scale)

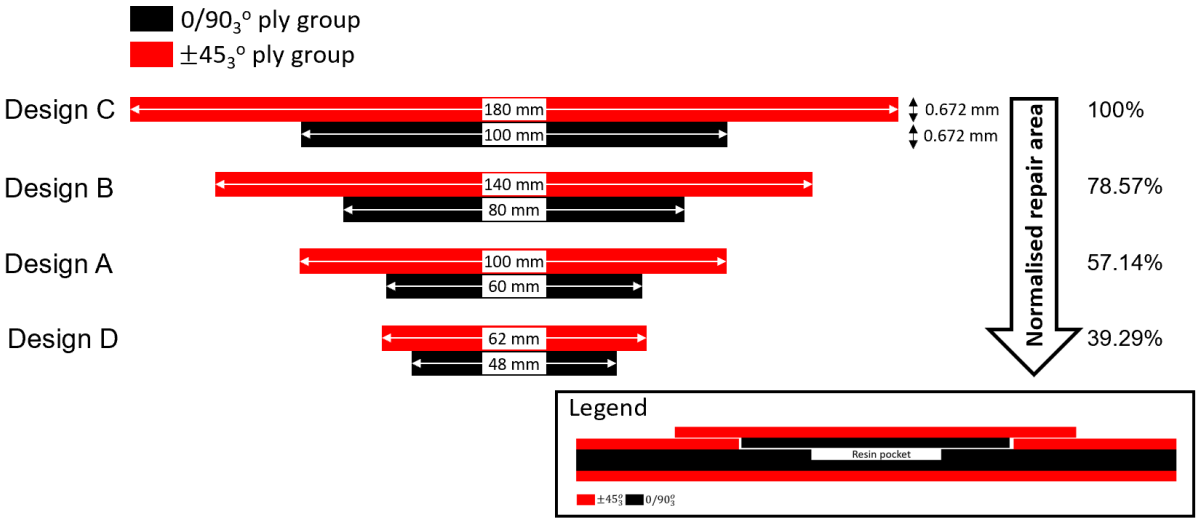

Figure 5: Illustration of repair plies for various repair designs with area of each repair normalised to that of Design C (drawn to scale horizontally but not through the thickness)

3.3 Finite element analysis (FEA)

The scarf step parameters β_1 and β_2 for design D were chosen via numerical FEA. At first, a progressive failure damage study (Quasi-static analysis) was carried out using the commercial Abaqus/Explicit software through a user-defined subroutine VUMAT on a pristine laminate with a symmetric and balanced stacking sequence of $[\pm 45_3, 0_3]_s$. The loaded end was given $4.5\,mm$ displacement using a smooth-step amplitude curve. For this study, the concept of using ply groups (cluster of plies with

similar orientation such as three plies of $0/90^o$ and three plies of $\pm 45^o$) was employed as it reflects the use of such stacks in the manufacture of future aircraft. The laminate was discretised using three dimensional 4-noded conventional shell elements with reduced integration scheme, i.e. S4R elements. The material damage model and damage parameters used in this study are comprehensively detailed in [24]. The purpose of progressive damage failure was to obtain the failure displacement, strain and load of the pristine laminate under pure tensile loading. Boundary conditions, loading and principal strain contour plots of the laminate are shown in Figure 6. The failure displacement, strain and force are predicted as $1.26\ mm$, 0.0125 and $26.67\ kN$, respectively.

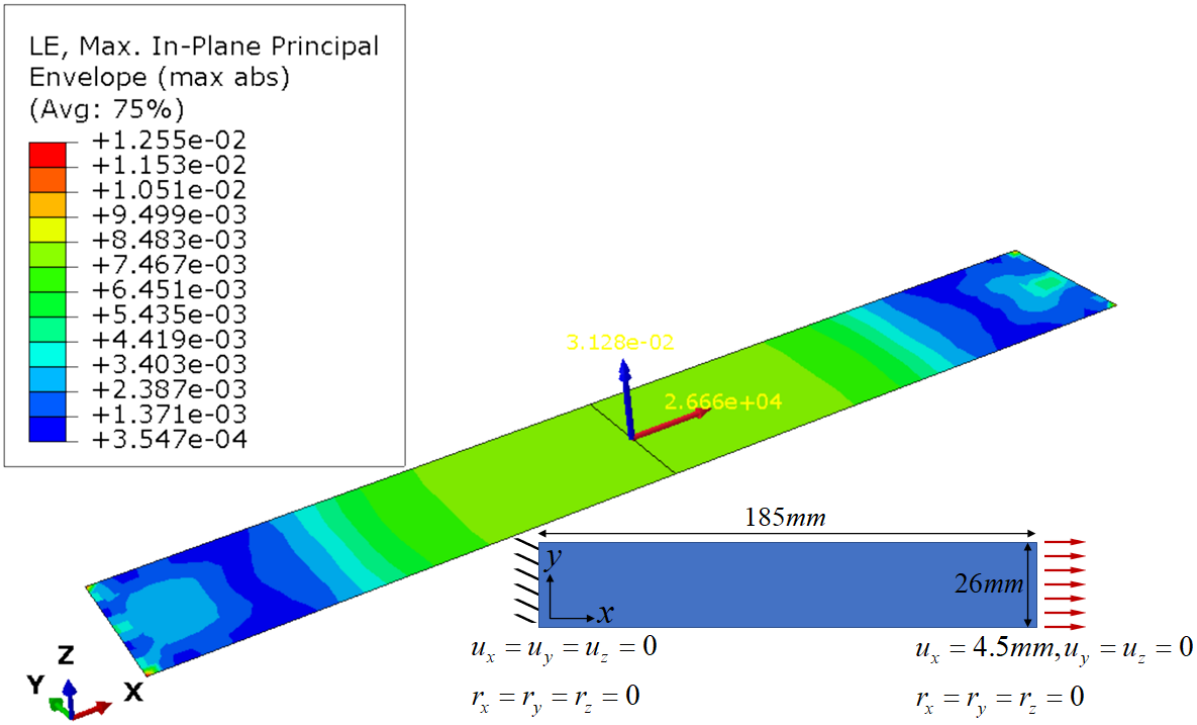

Figure 6: Predicted failure strain (0.0125) and failure force ($26.67\ kN$) of pristine laminate. (LE is logarithmic strain)

For the repair design, a static linear analysis of 2D plane strain finite element model was used. Due to symmetry of the structure, half of the displacement at failure ($0.63\ mm$) of the pristine laminate was applied to a half 2D plane stress model of the repair. Both the adherends and adhesive were modelled using linear 4-noded plane strain elements with reduced integration, i.e. CPE4R elements [25]. Figure 7 illustrates the boundary conditions, loading and mesh density of the structure. A fine mesh, with an element size of $0.08\ mm$, was adopted throughout the model. The adhesive was assumed to be $0.2\ mm$ thick and had three elements through the thickness.

Generally, there are five methods in the literature for designing bonded joints for laminated composite repairs. These methods are i) average stress method, ii) maximum stress method, iii) linear elastic fracture mechanics method, iv) virtual crack closure (VCCT) and v) cohesive zone modelling (CZM) techniques [5]. In this study, we apply an analysis approach which requires very limited FE model construction and execution time. Therefore, fracture mechanics and cohesive elements are not considered. An average stress design strategy is used to design the VLSS bonded repair. Although this criterion is strictly speaking valid only for joints between homogeneous materials of identical properties (such as metals), it has been chosen as a basis for comparison, because this technique is currently used in repair designs to size scarf repairs. Such a 'light' modelling strategy allows a design approach with low computational time (matching industrial practitioner needs) and herein will facilitate simple experiment/calculation comparisons.

To design the VLSS repair, β_1 and β_2 were continuously adjusted until the average shear stress along the mid-thickness plane of the adhesive layer was below the adhesive shear failure stress as shown in Figure A2d [23], [26]. The average shear stress for both the $\pm 45_3^o$ and the $0/90_3^o$ ply groups overlap was $8.01\,MPa$ and $9.16\,MPa$, respectively. These values are both below the shear stress allowable ($18\,MPa$ in Table A2) of the adhesive film. Section 2 of the Appendix (Figure A2) presents both the shear stress contour plots (τ_{xy}) within the adhesive and shear stress distribution along the mid-plane of the adhesive for all design configurations. In summary, with increasing overlap length the average shear stress decreases commensurately.

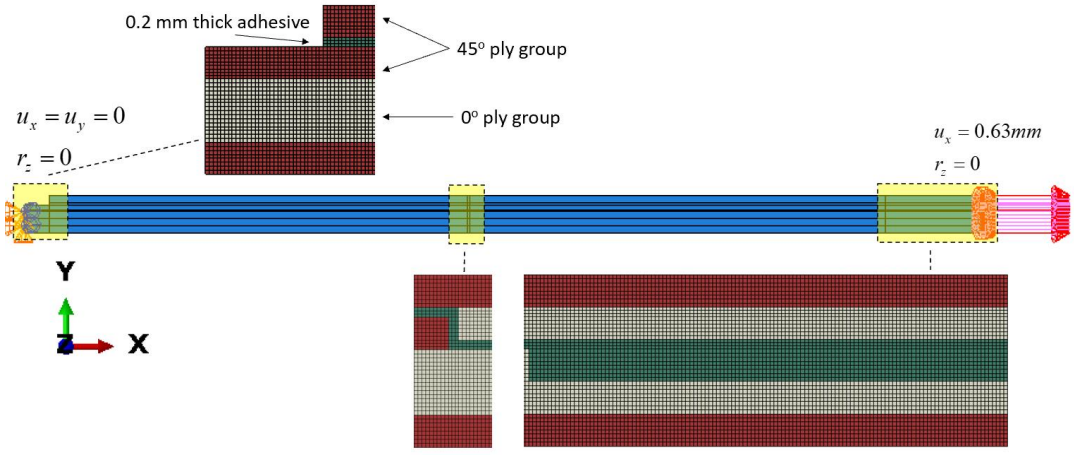

Figure 7: Boundary conditions and mesh illustration of 2D plain strain model of half the structure (shown for $\beta = 1/60$)

It is important to note that initially the repair design methodology was based on maximum shear stress criteria. This is because for joints bonded with brittle adhesives, it is believed that the maximum adhesive shear stress rather than the average shear stress will dictate the joint strength [23]. Hence, the use of average shear stress may over-estimate the joint strength. On the other hand, other works in the literature [21] suggest that both ends of the overlap will have a peak of shear stresses while at the midpoint of the bond-line the shear stress values will be close to zero (typical behaviour of bonded joints with brittle adhesives). For this reason, assessing the adhesive performance with the maximum shear stress is not useful. Close inspection of FEA results (Appendix - section 2) shows that even for the most conservative current industrial practice of $\beta = 1/60$, the maximum shear stress exceeds that of any available adhesive film in the literature [19], [27]–[29] and above the adhesive film properties used in this study, i.e. $18\ MPa$, confirming the arguments stated in [21]. However, the maximum shear stress in the proposed repair design scheme (Appendix - section 2) is significantly less than that of any standard repair, in particular 35% less than that of design C ($\beta = 1/60$).

Additionally, in some studies such as [10], [12], [30], [31], despite brittle behaviour of some adhesives, which is the case in this study, the von Mises stresses within the adhesive that are intended for ductile material are chosen as the failure criteria for the bonded joints. Despite the authors disagreement on such an approach due to brittle behaviour of adhesive material (Figure A1), investigation of peel stresses (Figure A3) and von Mises stresses (Figure A4) also indicate that design D benefits from less peel stress and von Mises stress compared to other repair designs. For all designs, apart from the edges, the peel stresses are almost zero within the adhesive. However, the von Mises stresses within the bondline are not bounded by the adhesive strength of $30\ MPa$ (see Figure A4) for any designs, even that of the most conservative and largest design C.

3.4 Repair preparation

Five laminates were manufactured, one for pristine specimens and four for designs A, B, C and D specimens. Each laminate had a lay-up $[\pm 45_3, 0_3]_s$ and was hand laid to form a plate and cured in a heated press for one hour at $120^o C$ under 100 psi pressure. The specimens were then abrasively cut to $185\ mm \times 185\ mm$ size.

The repair preparation, otherwise known as scarfing, can be achieved using existing technologies such as abrasive waterjet machining (AWJ), laser ablation and CNC milling as opposed to manual grinding [6]. It is worth noting that manual scarfing by skilled technicians is the current practice in both aerospace and in the wind turbine industries. For this work, a numerically controlled (NC) milling process was adopted. It should be noted that in the work of Psarra et al. [16], the use of laser cutting created a smoother surface but had only an improvement of 1% on the repair strength efficiency of the repaired laminate. Hence, in this study, for designs A, B, C and D, the samples were machined on a Bridgeport 600 vertical milling centre (Figure 8). A $10\,mm$ 4-flutes tungsten end mill was used, with a feed rate of $100\,mm/min$ with a spindle speed of $7500\,rpm$. The cutter paths for each sample profile were programmed using Featurecam computer-aided manufacturing software resulting in a raster path and a $0.2\,mm$ depth of cut per pass, until the required scarfing profile was achieved.

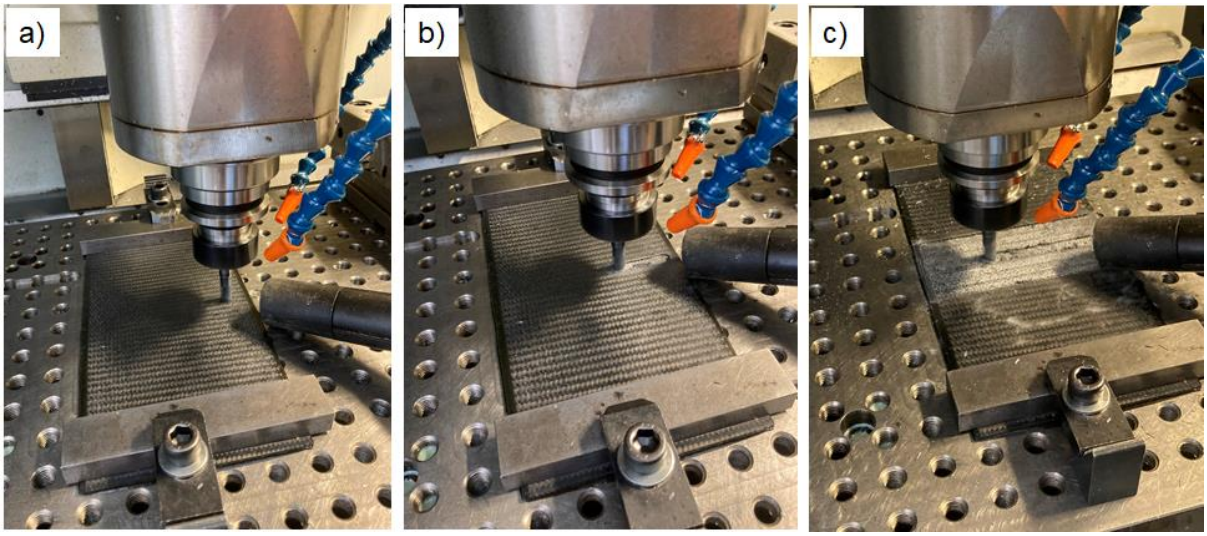

Figure 8: Progression of scarfing using CNC milling machine, a) start of scarfing, b) step scarfing of first ply group ($\pm 45_3^0$), c) step scarfing of the second ply group ($0/90_3^0$)

3.5 Machine vision and scarfing quality check

This section describes a novel imaging method to assess the quality and conditions of the scarf areas as implemented in section 3.4. For several decades, there have been many methods described in the manufacturing, image processing and computer vision literature to inspect non-composite components. Applications include methods for automated inspection of components and raw materials at varying scales. However, standard imaging techniques suffer in the case of carbon composite materials inspection due to their awkward, black and shiny appearance. This difficulty

is exemplified by Figure 9a which shows a standard greyscale image of a woven CFRP surface under dome (omnidirectional) illumination. Given the difficulty in human assessment of this image, let alone that for *automated* analysis, even in the ideal lighting, it is unsurprising that successes in automated visual assessment of CFRP has been limited.

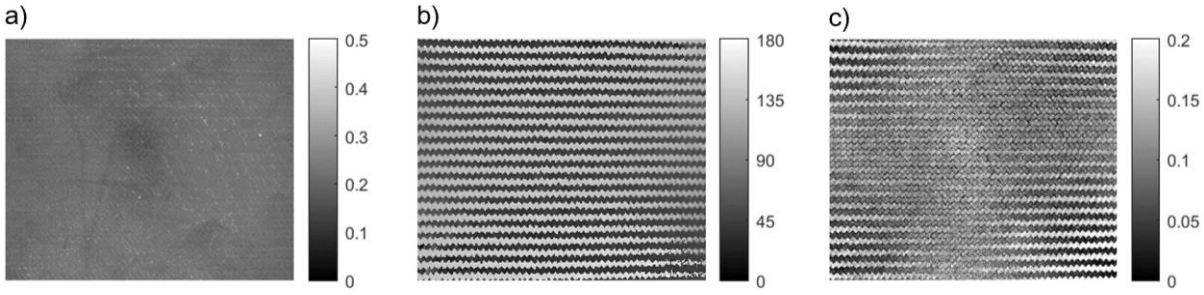

Figure 9: Polarisation image of a planar (unscarfed) woven CFRP component, a) Intensity, b) AoLP, c) DoP. These data were captured using the Sony XCG-CP510 camera with a $12\ mm$ lens under a $300\ mm$ diameter, blue ($465\ nm$) LED dome lighting.

To overcome the imaging difficulties discussed above, this paper makes use of a recently commercialised "polarisation camera" developed by Sony. The field of "polarisation vision" [32] aims to assess the polarisation state of light entering a camera to deduce information about the region being imaged. Often, the state of this light is parametrised by three values:

- *Intensity*: this is simply a measure of brightness at each pixel and is identical to that which can be found in a standard monochrome camera.
- *Phase* or *angle of linear polarisation* (AoLP): this corresponds to the angle of the principal electric field of the incoming light wave.
- *Degree of polarisation* (DoP): this determines whether the light is unpolarised (with a value of 0), completely linearly polarised (1) or partially polarised (in-between values). Note that elliptical polarisation is not modelled in this formulation.

In this paper, we are primarily concerned with the AoLP. That is because any unpolarised light that is incident on a carbon fibre will be reflected such that the AoLP will be aligned with the fibres [32], [33]. This is exemplified in Figure 9b, where the woven layup structure is much more visible than in the standard intensity image.

The AoLP images for all four test designs A – D are shown in Figure 10 using a colour mapping to enhance the appearance of the fibre orientations. The images

clearly demonstrate the layup structure and interfaces/steps of the scarf. It is worth noting that in a few cases, the milling process has been unsuccessful in completely penetrating a layer, and this is immediately apparent from the images - most notably, the upper part of image (c). These figures demonstrate that scarfing penetration is executed with reasonable precision for design A, B and D. However, as shown in Figure 10c, scarfing of design C did not penetrate fully through $\pm 45_3^o$ ply group within the $1/3$ top portion of the laminate.

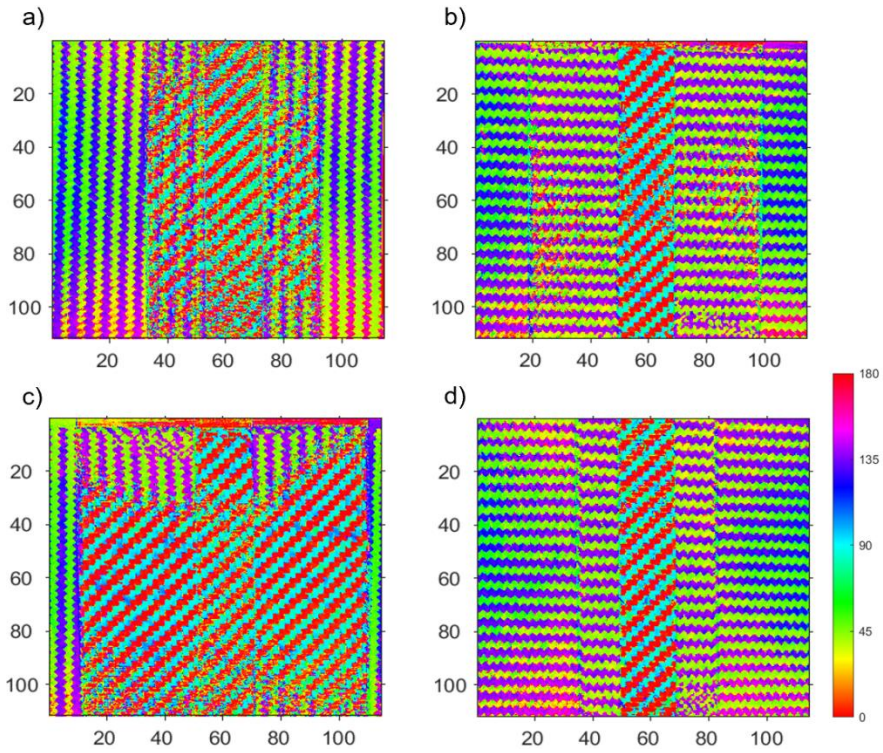

Figure 10: AoLP images for each repair design A, B, C and D. Axis units are in mm, colour encodes fibre angle according to the scale on the right.

The final step of the machine vision part of the paper is to extract numerical data from Figure 10. To do this, the histograms of orientations are plotted for each step in the scarf. By way of example, the histograms for a region to the far left of Figure 10d and the central area of Figure 10d are plotted in Figure 11. This shows the capability of machine vision in obtaining ply orientation of scarfed plies. This is a potentially crucial step since it is often difficult to verify whether a full layer has been removed by other means – especially in the less controlled cases of grinding out scarfs. The combination of AoLP images and histograms give evidence of the underlying integrity of the component before testing or patch repair.

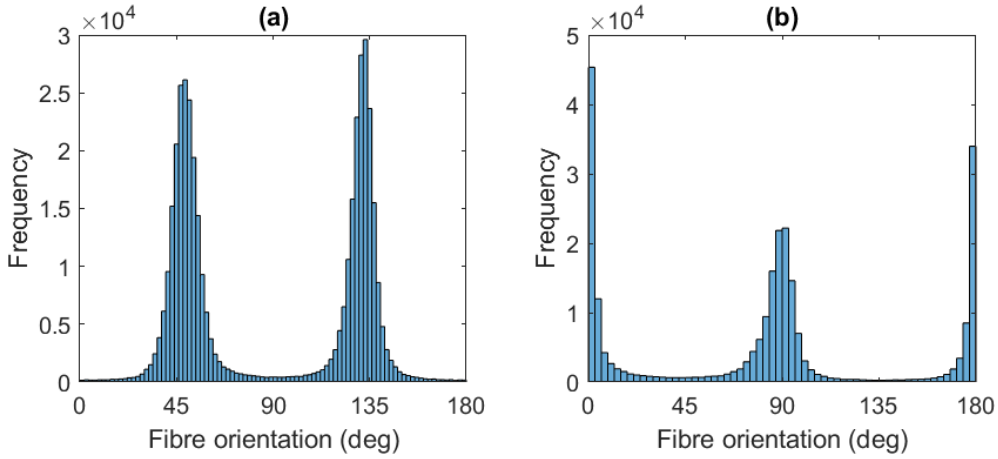

Figure 11: Histograms of ply orientation, a) far left and b) central steps from Figure 10d

3.6 Repair manufacture

The scarfed area of laminates were sanded manually using 240-grit sandpaper and degreased and cleaned using alcohol and acetone. The choice of a coarse sand paper was based on literature and the notion that sandpaper granularity has an indirect correlation with the quality of the repair bond, i.e. a courser sandpaper could lead to a better bond between the repair and the parent laminate [34]. The repair process was composed of different phases. First, the adhesive film of XA120 was placed in the stepped-lap area. Then, the repair plies were stacked, for the first ply group $(0/90_3)$ to the second repair ply group $(\pm 45_3)$. Once all the repair plies were laid up, a vacuum bag was installed and sealed. Then, a vacuum test was performed to ascertain pressure would be applied on the laminates throughout the curing process. The vacuum was applied using an external pump. The vacuum bag with the repaired laminates were then placed on the press machine, not for pressure but for the heating component of the press machine (see Figure 12). The heated press was set to $120^o C$ as this was the curing temperature of the adhesive film and was left for 1 hour and a further 1 hour for post cure. Figure 13 shows how this process was executed.

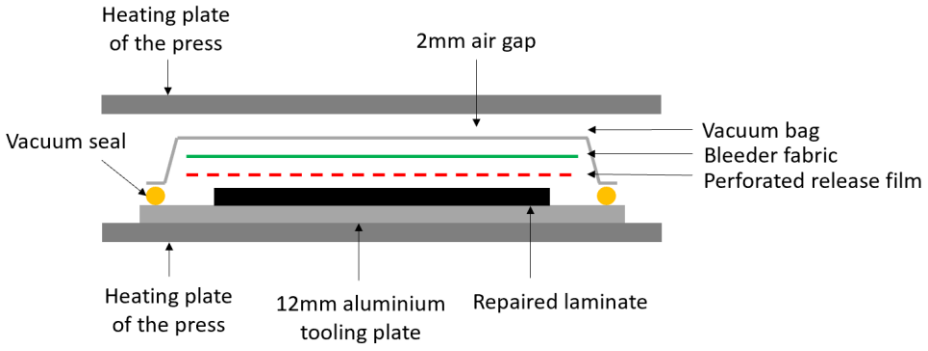

Figure 12: Schematic of vacuum process for laminate repair

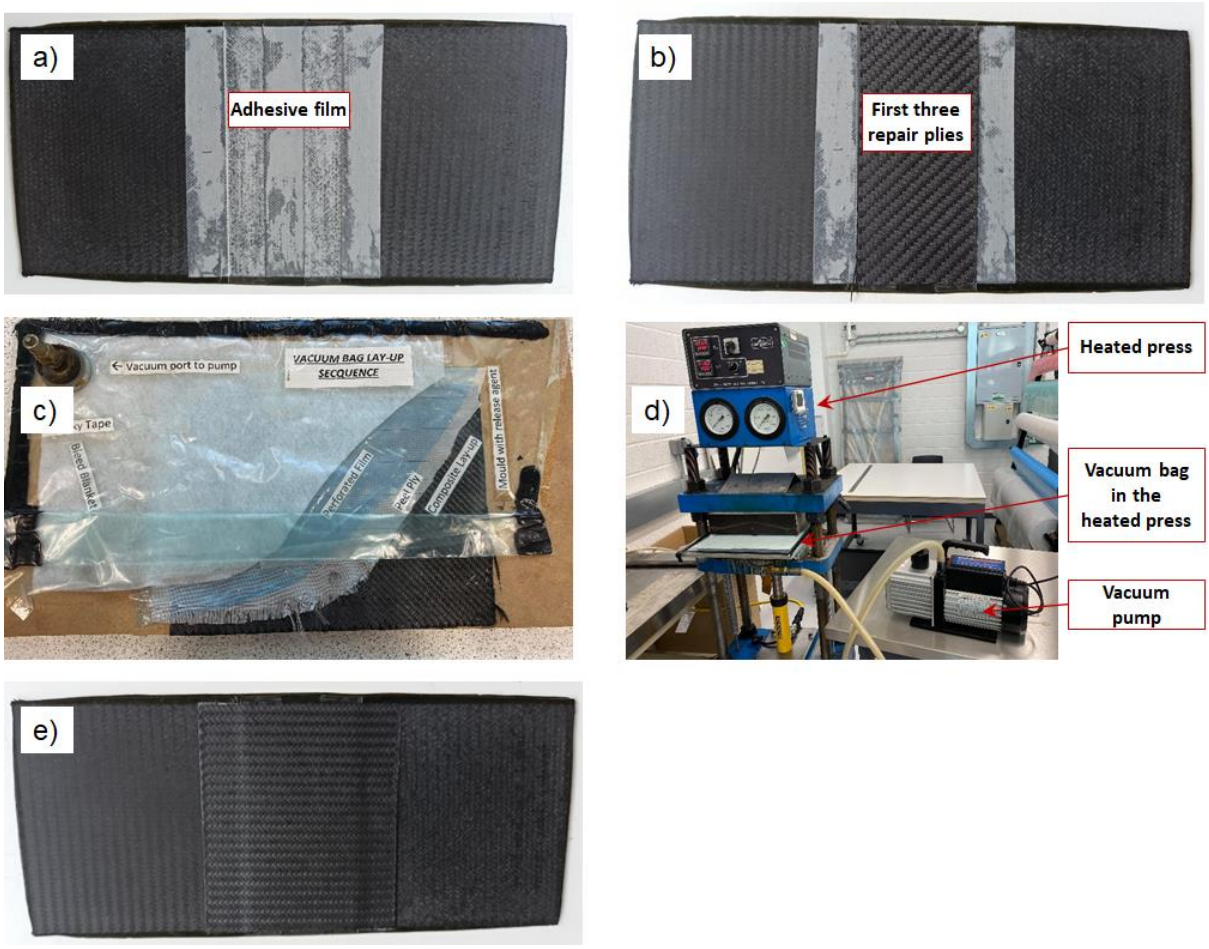

Figure 13: Overview of the repair process, a) lay down of XA120 adhesive file, b) placing the first three $(0/90_3^0)$ repair plies, c) vacuum bag set-up, d) placement of vacuum bag in the heated press, e) repaired laminate for design A $(\beta = 1/30)$

3.7 Mechanical testing

Each repaired laminate was cut into $26\ mm$ wide tensile coupons (see Figure 14a). To have statistically repeatable data, three coupons for each repair design were tested in tension using a $100\ kN$ capacity INSTRON tensile machine at a speed of $2\ mm/min$. It should be noted that, unlike repaired laminates, nine pristine laminates were tested. One of such coupons for each repair design was strain gauged at 5 locations as shown in Figure 14b, i.e. just before and after the bond-line and in the middle of the repair. The strain gauges had grid resistance of $120.0 \pm 0.3\%\ Ohms$. The other two coupons were not strain gauged and instead had an extensometer attached to the mid-length of the coupons (see Figure 14c). It should be noted that the extensometer was removed at a set strain level (≈ 3000 μstrain) before the failure of the test coupons to avoid extensometer damage. From the point of removal, the strain readings were obtained by the machine based on crosshead movements and considering unavoidable compliance in the machine, load cell and grips. The choice

of strain gauging strategy was to monitor the flow of strain from the parent laminate to the repair patch. In the case of Design C, due to imperfect scarfing (see Figure 10c), the three tensile coupons were obtained from the portion with precise scarfing as determined by the machine vision process. However, one coupon from the imperfectly scarfed portion was tested and labelled as design C' to understand the impact of imperfect scarfing on the repair efficiency.

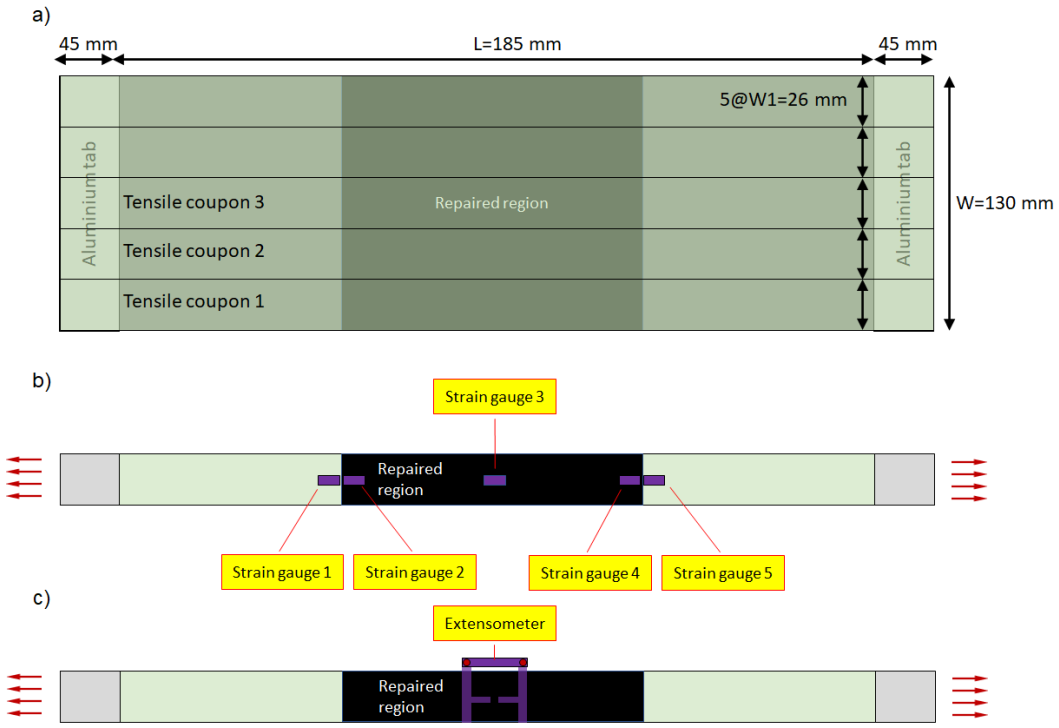

Figure 14: Overview of the tensile coupons cut from repaired laminates, a) tensile coupons, b) strain gauging strategy for one of coupons, c) extensometer location for two of coupons (not shown to scale)

4 Results and discussions

The force-displacement graphs for the pristine/intact and repair designs A-D are shown in Figure 15. It is evident that force-displacement behaviour of both the pristine and repair laminates are almost linear with a sudden abrupt failure typical of CFRP laminated composite structures. There is a kink at $\approx 0.6\,mm$ displacement for all test coupons including the pristine ones that derives from a characteristic of the test set-up resulting from settling of end fixtures during loading. Furthermore, during the testing of the specimens, a common trend was observed. After the initial linear behaviour, at a certain load level there was a small load drop for pristine laminates at $\approx 3.5\,mm$ displacement. However, for repaired specimens, there were three small load drops for design A (Figure 15b) and two small load drops for other designs at various

displacement levels (Figure 15c-f). These load drops are the manifestation of the formation of initial small scale inter and intra lamina damage within the test specimens. For instance, the drop for pristine laminates are associated to the formation of cracks and delamination between $0/90_3^o$ and $\pm 45_3^o$ at the free edges as reported in [16]. On the other hand, the load drops for the repaired specimens are associated to a combination of adherend-adhesive interfacial debond, formation of delamination and its growth as will be discussed later in this section. It is observed that after load drops the slope of the force-displacement graph (Hooke's axial stiffness) does not significantly change. A summary of failure loads, failure displacements and Hooke's axial stiffnesses for all the repair designs are tabulated in Table 2. Additionally, the repair efficiency parameters for failure loads, failure displacements and Hooke's stiffnesses are normalised to those of the pristine coupons and are illustrated in Figure 16. The average Hooke's axial stiffness of the pristine laminates is $6603.8\,MPa$. Generally, all repair designs restore more than 90% of the pristine Hooke's axial stiffness. Interestingly, the smallest repair design D restores 95% of Hooke's axial stiffness compared to the largest repair design C with 91.4% stiffness restoration. This could be associated with removal of a smaller volume of healthy material in design D compared to design C. On the other hand, the experimental data also suggests that larger β values result in less strength efficiency. Obviously, this contrasts with the behavior seen in the simulation results, where larger β values result in less joint stresses (both in terms of maximum shear and peel stresses). This contradictory behaviour may result from a greater difficulty in achieving a quality bond when the individual length of each step size is decreased. Furthermore, this contradiction indicates that failure criteria based on average shear stresses are more suitable than maximum shear stresses for integrity assessment of bonded repair. For instance, the average shear stresses within the adhesive for the most load carrying plies ($0/90_3^o$) are $3.87\,MPa$ and $9.16\,MPa$ for design C and design D, respectively. This is a 42% reduction in average shear stress for design C compared to design D which could be a contributory factor to an enhanced strength efficiency of the largest repair.

To understand the effect of imperfect scarfing on the repair efficiency, Figure 15e shows that the repair associated to the imperfect scarfing (repair C') has an overall failure load of $22.12\,kN$. This failure load when compared to the $23.32\,kN$ load of the correctly scarfed specimens (repair C) of Table 2, shows an almost 5% reduction. The

impact on Hooke's axial stiffness was only reduced by 1%. Hence, in this case, the imperfect scarfing had only a modest effect on the overall repair efficiency.

It is worth noting that the variation seen in the results of design B is notably greater than seen in the other designs. However, the magnitude of variation does not appear significantly greater than that of the pristine specimens, where a total of nine repeat tests where undertaken. It is also worth noting that each repeat specimen was sectioned from a single laminate, which was processed as a single repair instant. Thus, the variation in the structural measurands does not capture the repair process repeatability, but the variation in the structural performance along a single repair plane.

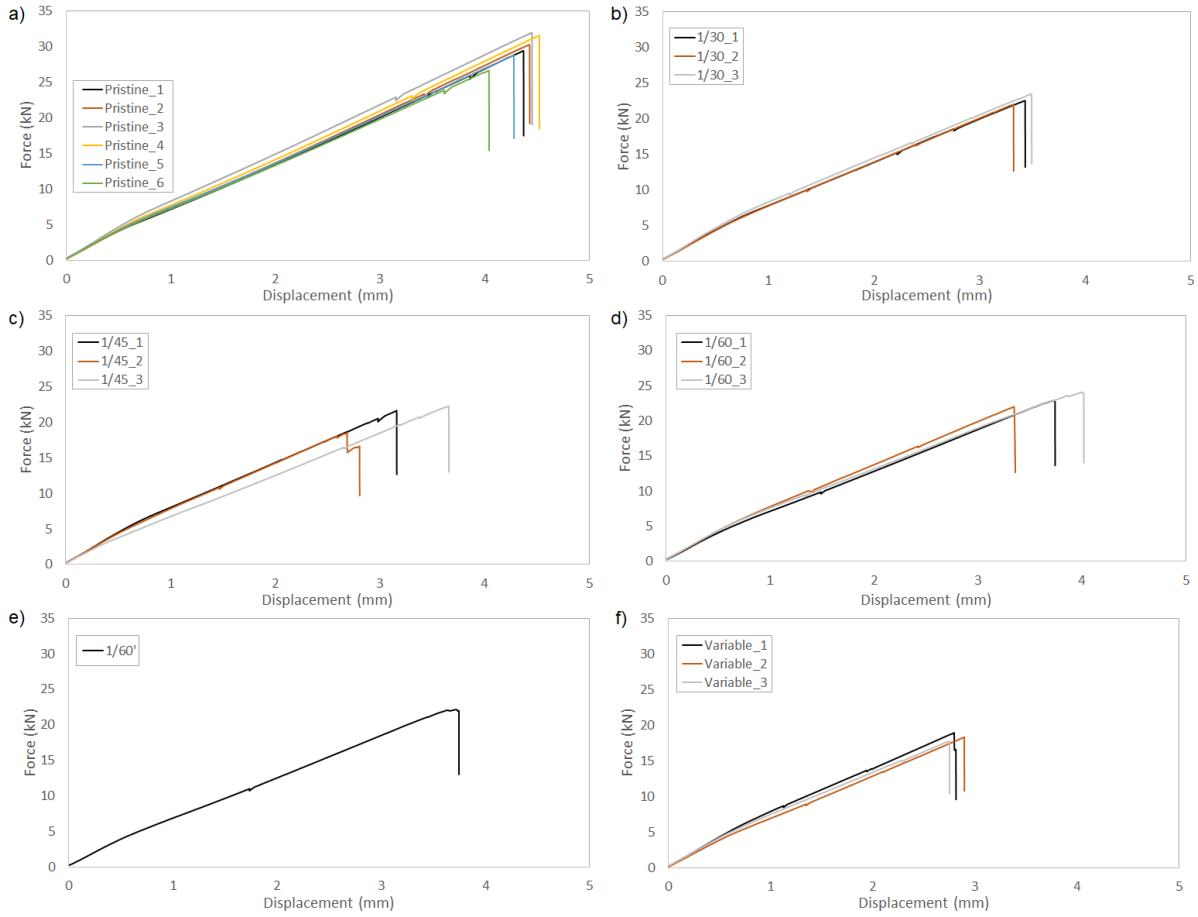

Figure 15: Force-displacement graph of, a) pristine coupons (shown for 6 laminates only), b) repair design A coupons, c) repair design B coupons, d) repair design C coupons, e) repair design C' coupon (imperfect scarfing), f) repair design D coupons (VLSS)

Table 2: Summary of test outputs from force-displacement graphs for all repair designs

Repair design	Scarf step parameter β_1, β_2	Area of material removed (mm^2)*	Failure Load (kN)	Failure Displacement (mm)	Hooke's axial stiffness (N/mm)
Pristine	N/A	N/A	29.16 ± 2.00**	4.31 ± 0.20	6603.82 ± 262.26
A	1/30,1/30	107.52	22.44 ± 0.75***	3.39 ± 0.09	6363.23 ± 54.81
B	1/45,1/45	147.84	20.80 ± 2.02****	3.20 ± 0.43	6371.43 ± 396.79
C	1/60,1/60	188.16	23.32 ± 0.66****	3.92 ± 0.16	6035.13 ± 244.09
D	1/20,1/10	73.92	18.66 ± 0.31****	2.82 ± 0.07	6277.53 ± 262.26

* per unit of width
** standard deviation for 9 tested specimens
*** standard deviation for 4 tested specimens
**** standard deviation for 3 tested specimens

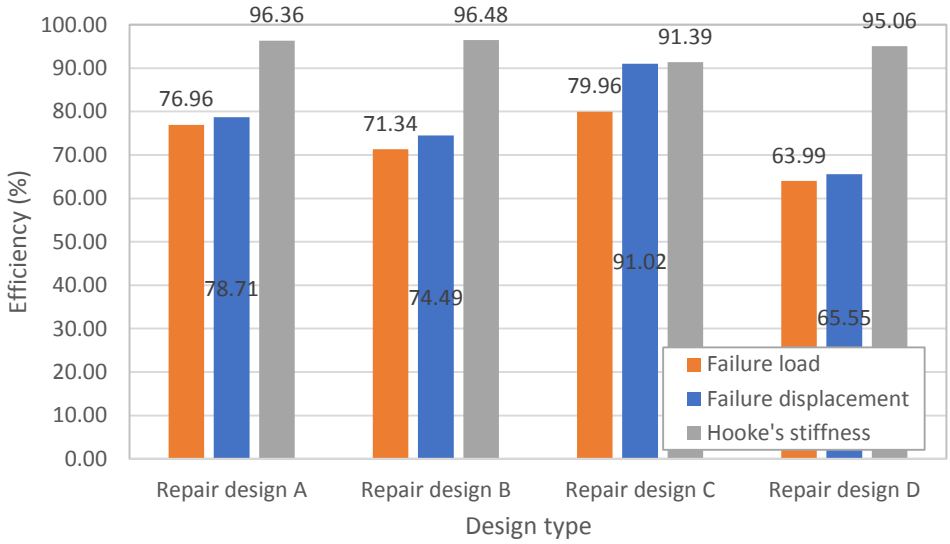

Figure 16: Average repair efficiency parameters normalised to those of pristine coupons (see Figure A5 for scattered data)

Investigation of the failure mechanisms for the specimens shows that the failure of repair designs A and D was the same. As can be seen in Figure 17 (shown for repair D) and Figure 18 (shown for repair A), the failure process was associated to the debond of the repair patch from the parent laminate (adherend-adhesive interface). With failure initiated from the locations of point 4 at interface 2 (see inset of Figure 17) and later from point 1 at interface 1 (at the end of the cut ply close to the loaded end). This is expected as the $0/90_3^o$ ply group transfer much higher end loads compared to the $\pm 45_3^o$ ply group. The same form of adhesive-adherend interfacial debond failure within the steps was reported in the work of Psarras et al. [16]. After the initial failure the debonds spread in the direction of points 3 and 2 from point 4 and 1, respectively. Throughout the failure process, delamination of the repair plies was observed as

shown in Figure 17. This observation is in agreement with the findings in the work of Truong et al. [36], where interlaminar shear stresses led to delamination of the repair patch in a stepped scarf repair. Referring to contour plots of interlaminar shear stresses of FigureA2.a and FigureA2.**Error! Reference source not found.**d, the epair patch experiences elevated interlaminar shear stresses (orange contours at the step location of point 4) within the $0/90_3^o$ repair plies and the interface between the $\pm 45_3^o$ and the $0/90_3^o$ repair plies. This stress state will have contributed to the formation of the delamination and progression via fracture mode I and II, due to the elevated peel (S_{22}) and interlaminar shear stresses (S_{12}), respectively. No delamination within the $\pm 45_3^o$ repair ply group took place. It should be noted that, during the failure process the cohesive failure of the adhesive was not observed in these repairs (see Figure 17). Generally, the free edge locations (point 4 and point 1- yellow line of Figure 17) experience higher shear and peel stresses as shown in the numerical study of section 3.1 - which leads to the formation of cracks and failure of the adhesive-adherend interface through crack propagation in fracture mode I and II [37]. After the debond, overall failure of the test laminates for these designs took place immediately in the form of fibre failure (adherend cohesive failure) of the parent laminate in the middle of the test coupon.

As shown in Figure 19, failure behaviour of repair design B demonstrated a more desirable failure process. In other words, the debond started at point 4 of interface 2 and started growing towards point 3. The debond then spread onto interface 1 starting at point 2. Subsequently, fibre failure of the parent laminate took place. It is noted that the debond never spread up to point 1, throughout the failure process, and delamination within the 0_3^o repair plie group and at the interface between the $\pm 45_3^o$ and the $0/90_3^o$ repair ply groups was present throughout the failure process. In this case, no delamination was observed within the $\pm 45_3^o$ repair ply group. Similar to designs A and D, the existence of delamination is associated to elevated interlaminar shear stresses in the repair patch at the location of steps (point 4 in particular). Once again, based on Figure A2, point 4 experiences the highest shear stress and is expected to be the location of initiation of failure.

The most conservative and the largest repair design (C) demonstrated the most desirable failure behaviour in which the load was fully transferred through the adhesive into the repair patch. In this repair, adhesive-adherend debond at interface 2 was

followed by fibre fracture of the repair which was then immediately succeeded by sudden fibre fracture of the parent laminate as shown in Figure 20. Unlike repair designs A, B and D, no delamination of repair plies took place. These observations happened despite higher numerical interlaminar shear and peel stresses in repair design C compared to the other repairs particularly those of repair design D. However, the average shear stress within the adhesive in design C is less than that of design D. This indicates that the average shear stress is responsible for the failure of the bonded joint rather than the maximum shear stress. As mentioned in section 3.3, it could be argued that point stress criteria (peak shear stress, von Mises or Tresca failure criteria) are not suitable for assessing the integrity of bonded joints in laminated composite structures. Besides, the absence of adhesive cohesive failure, delamination of repair ply groups and the dominance of interfacial debond (in all repairs particularly in repair designs A and D), points to the well-known underperformance of interfacial bond and the difficulty of certifying them for use in aircraft primary structures. In fact, not only are there shortcomings and challenges to create a perfect bond between adherend and adhesive but also it is difficult to implement a repair with consistent bond strength over a large area. There have been many attempts in the literature to improve interfacial bonds in bonded composites such as bond surface treatment using laser [38], but this topic is beyond the scope of this study and hence not explored further. From the findings mentioned above, it is suspected that since the overlap length for designs A and D are small, it is possible that the pressure from the vacuum process was less efficient in creating bonds of designs B and C. Hence, the manufacturing as used for large repair may not be suitable for smaller repairs. It should be noted that, in practice, obtaining a good distribution of pressure and heat when curing a repair on aircraft primary structure is hard enough without making the repair area large and encompassing a complex shape.

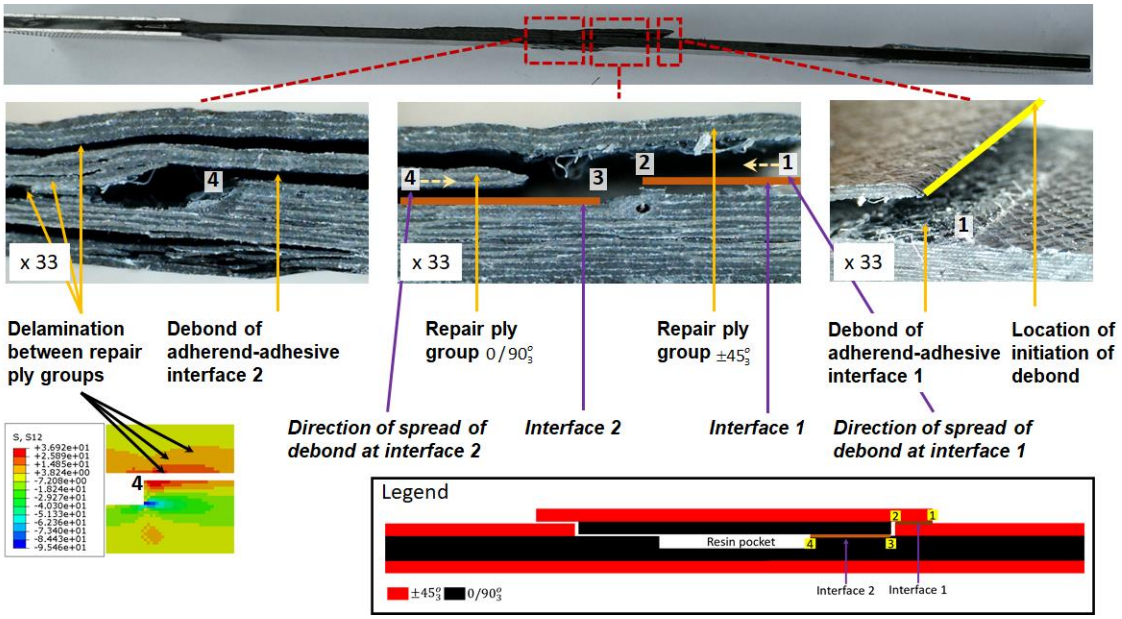

Figure 17: Magnified view (× 33) of failed specimen for repair design D

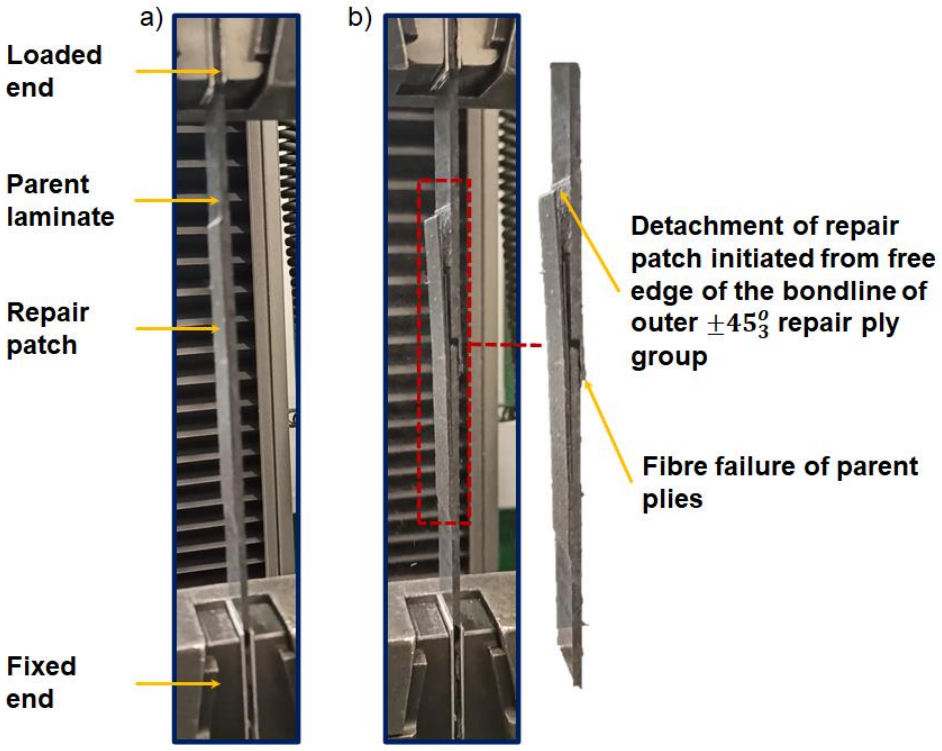

Figure 18: Failure process of repair design A throughout the test, a) at the start of the test, b) debond of repair patch initiated from free edge of adherend-adhesive interface for outer $\pm 45^{o}_{3}$ repair ply group

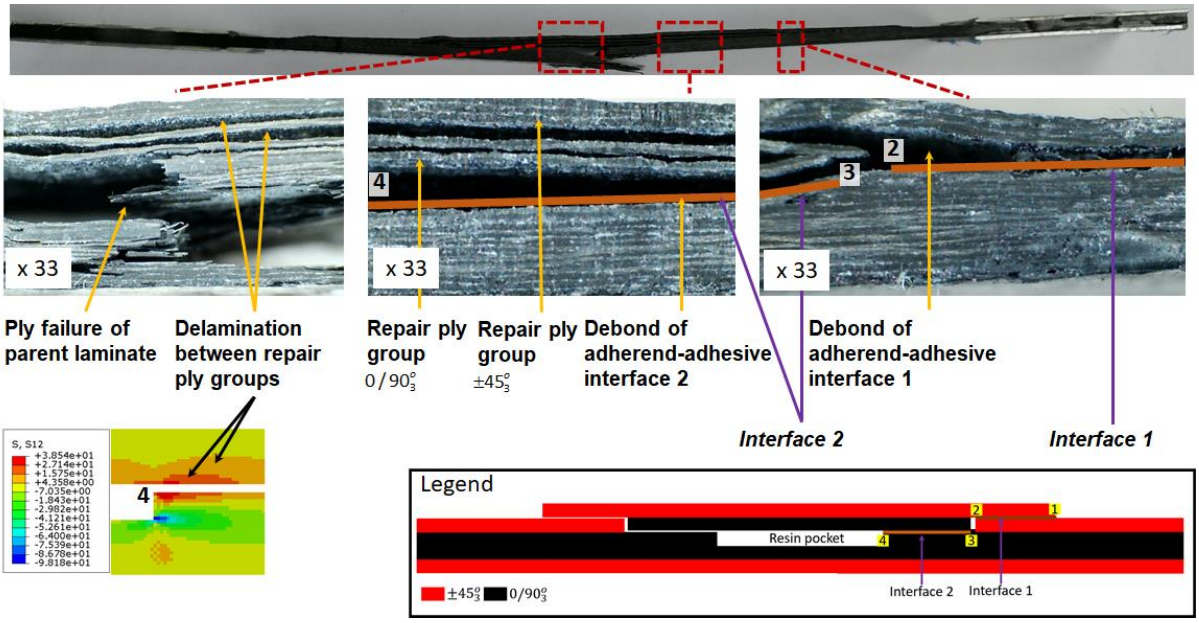

Figure 19: Magnified view ($\times$ 33) of failed specimen for repair design B

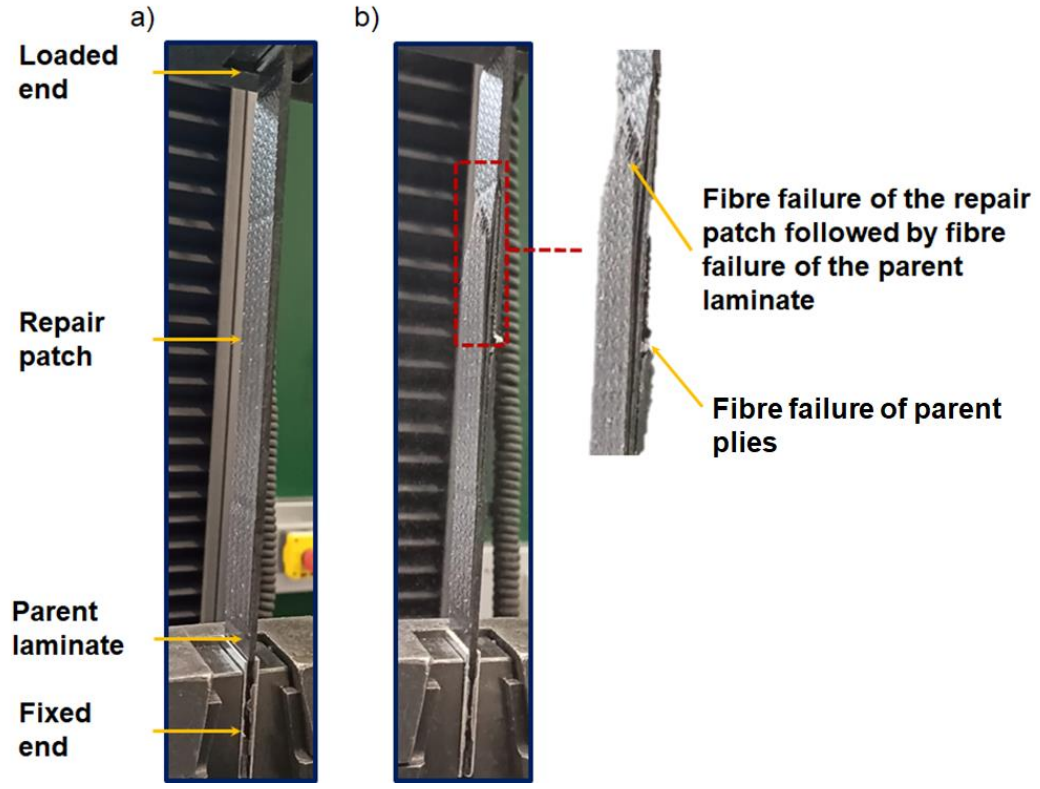

Figure 20: Failure process of repair design C throughout the test, a) at the start of the test, b) fibre failure of repair patch in the middle of the test coupon followed by fibre failure of the parent laminate

Figure 21 shows stress-strain curves for the five strain gauges for the gauged specimens. A summary of stress-strain data obtained from both strain gauges (failure strains) and extensometer readings (failure stress) is tabulated in Table 3. It is evident from the graphs that in all repair designs and for any given load/stress, the strain

gauges on the parent laminate side (gauges 1 and 5) show much higher strains compared to those on the repair patch side (gauges 2 and 4) owing to the asymmetry and offset of the neutral axis introduced by the lap repair. As load increases so does the difference between the strain gauge readings on the repair patch and those on the parent structure. This is due to the repair patch becoming less functional as a result of initiation of nonlinearity within the repair patch. i.e. interfacial debonding and delamination. This strain discrepancy increases nonlinearly, peaking close to the final failure. Figure 22 shows the principal stress contour plots from FEA for the scarfed laminates at $0.63\,mm$ imposed displacement load level. This figure can be used to understand the coupons behaviour once the repair detaches from the structure, which is at the time close to final failure of the coupons. As the repair detaches/fails and becomes fully dysfunctional in the loading process, very high stress concentrations (with stress concentration factors (SCF) of $8.89 - 9.00$) take place for the most load carrying parent plies ($0/90_3^0$ plies) at the location of point 4. This observation is in agreement with those of [39]. These high stresses are responsible for immediate failure of the parent laminate after the repair patch fails – with section failure location along the prismatic section of the parent material possibly dictated by ply imperfections. Moreover, close to the time of failure, the complete change in load path from fully functional repaired structure to scarfed structure leads to maximum discrepancy between the strain readings on the repair patch and those on the parent structure.

Based on Table 3, as the repair β values increase, the specimens experience higher strains but never manage to match those of the pristine laminates (12376 μstrain). This is due to the failure of the repair patch after which the load path changes requiring the scarfed laminate to carry the entire load. As shown in Figure 16, due to the asymmetry of the scarfed laminate and hence the load eccentricity, bending and out of plane displacement of the scarfed laminates takes place [7]. This is also likely to reduce the specimens ultimate strength and match the strains equivalent to those of the pristine laminates (at least at the location of the strain gauges). In interpretation of stress-strain data, one should note that the decrease of the repair size is accompanied by simultaneous decrease in section membrane forces and increase in section bending moments (see Figure A6). This leads to strain readings to be a combination of both axial and bending strains for repaired specimens whereas in the

pristine specimens the strain readings are associated to pure tension loading only (with no load eccentricity hence no section bending moments). As such, homogenised Young's modulus (slope of stress-strain test data) are not an exact like for like comparison with that of pristine laminates and hence not provided in this study.

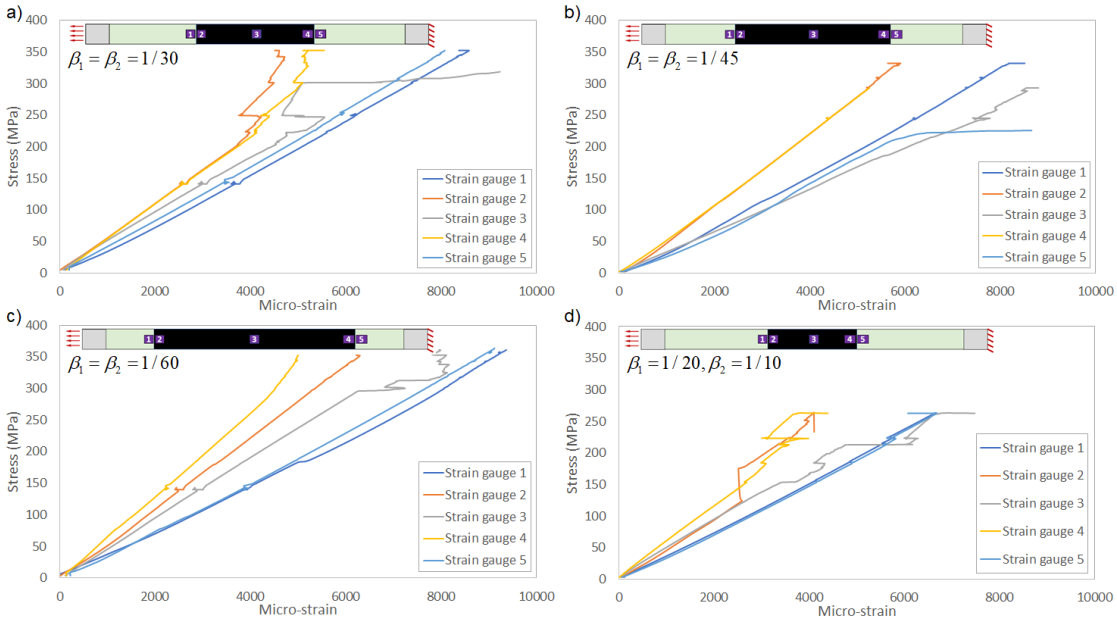

Figure 21: Stress-strain curves for five strain gauges, a) Repair design A, b) Repair design B, c) Repair design C and d) Repair design D (VLSS)

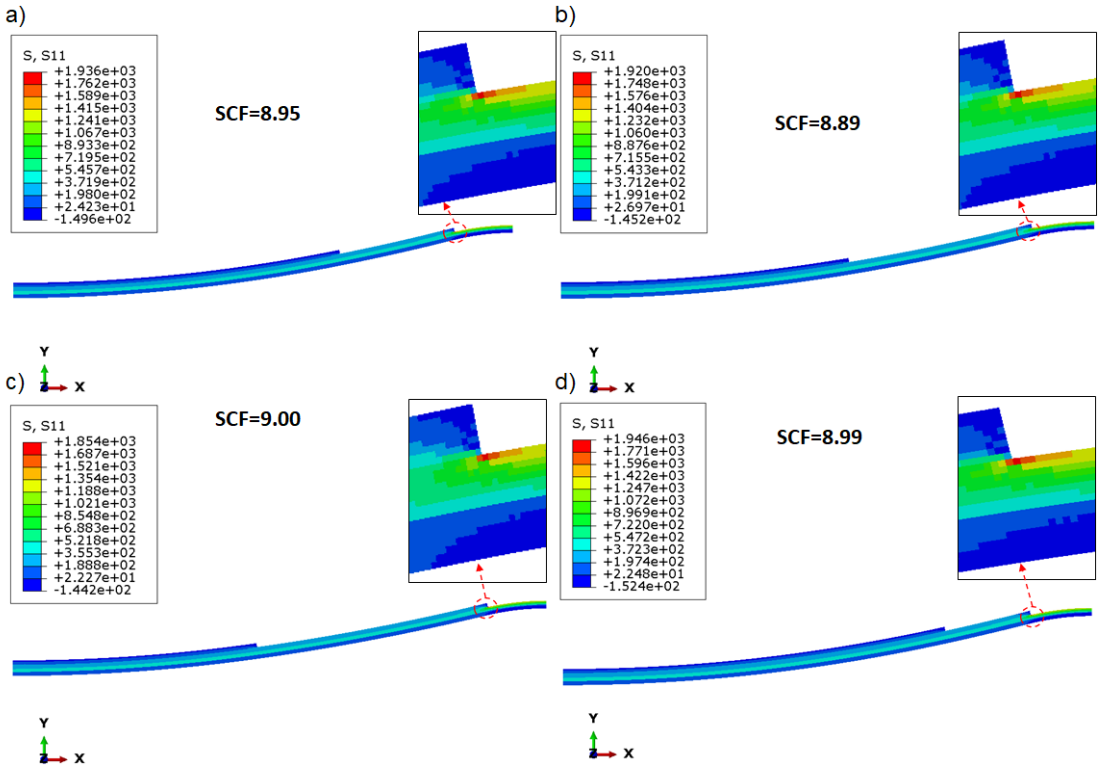

Figure 22: Principal stress contour plots (in direction x) of scarfed laminates for enforced displacement of $0.63\ mm$, a) repair design A, b) repair design B, c) repair design C and d) repair design D (SCF is stress concentration factor and all units all in MPa)

Table 3: Summary of test outputs from stress-strain graphs for all repair designs

Repair design	Failure stress (MPa)**	Failure strain (μstrain)*
Pristine	440.67 ± 15.58	12376.00
A	353.12 ± 11.11	8314.00
B	316.43 ± 22.84	8581.00
C	346.96 ± 12.09	9360.00
D	280.56 ± 14.11	7482.00

* no standard deviation available as these are averages of strain gauges 1 and 5 (on the parent laminate side)
** obtained from tensile machine for all specimens

5 Conclusions

A detailed design of a stepped scarf repair for highly loaded composite structures based on numerical linear FEA has been presented. A novel VLSS design for minimum size has been introduced. The performance of VLSS (or known as repair design D in this study) as well as three other established stepped scarf repair designs has been evaluated experimentally. Laminate preparation and scarfing has been executed using a numerically controlled milling process. For the first time, the quality of scarf has been inspected by machine vision. The experimental results show that the VLSS repair scheme was able to demonstrate $\approx 95\%$ stiffer behaviour compared to the largest repair scheme of 91.4%. This is beneficial where stiffness restoration is crucial, for example when buckling is a critical design constraint. However, VLSS fell short in restoring the static strength of the structure. In fact, its strength repair efficiency (64%) was the lowest of the examined repair designs, owing to underperforming adhesive-adherend interfacial bond strength. Repair design C (with overlap length of $\beta = 1/60$) showed a superior repair strength efficiency $\approx 77\%$ compared to the other repair designs and demonstrated a desirable failure response, i.e. fibre fracture in both repair patch and parent laminate as opposed to failure within the adhesive-adherent interface. For all repairs except for repair design C, the failure process was associated to adhesive-adherend interfacial debond and delamination of the $0/90_3^o$ repair ply groups immediately followed by cohesive failure of the parent plies in the middle of the test coupons. Further study is required to improve the bond strength between the repair patch and the parent laminate to diminish the undesirable failure process through the adhesive-adherend interface. A detailed progressive failure analysis based on fracture mechanics (cohesive zone modelling) could benefit the repair design and provide further insight into the damage mechanisms of the studied designs.

The effects of laser cutting on the quality of prepared laminate as opposed to machine milling on the repair efficiency needs to be studied. Additionally, the behaviour of these repairs need to be investigated under static shear and compression loading, fatigue and impact loading.

Acknowledgement

The authors express their gratitude to Douglas Nash, Mark Allonby and Daniel Cole (technicians at UWE) for their assistance and facilitating the research during the COVID-19 pandemic.

Appendix

1 Specimen mechanical properties

Table A1: Mechanical properties of both woven CFRP (AX-5180) fabric plies [24]

Mechanical properties	Units	AX-5180 CFRP
$E_{11}=E_{22}$	MPa	67094.00
G_{12}	MPa	4831.38
S_t^*	MPa	595.50
S_c	MPa	393.00
S_s	MPa	87.00
Strain to failure	Strain	0.014
ϑ_{12} (Poisson's ratio)	N/A	0.04
t_{ply}**	mm	0.224

Table A2: Mechanical properties of adhesive film XA120 (tensile test is done in-house)

Mechanical properties	Units	AX-5180 CFRP
E	MPa	1644.00
G*	MPa	610.00
S_t	MPa	30.00
S_s**	MPa	18.00
ϑ_{12} (Poisson's ratio)	N/A	0.35

* estimated from $G = E/2(1+\vartheta_{12})$ based on [29]
** approximated from $0.5S_t + \mu$ for brittle adhesives where μ is taken as an average of data from [19], [27], [40], [41]

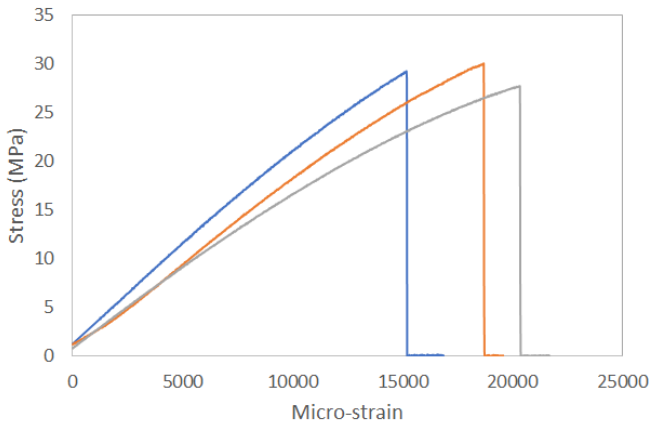

Figure A1: Stress-strain curve of tensile test of adhesive used in the study (XA120) showing an almost brittle failure

2 Repair design simulation results

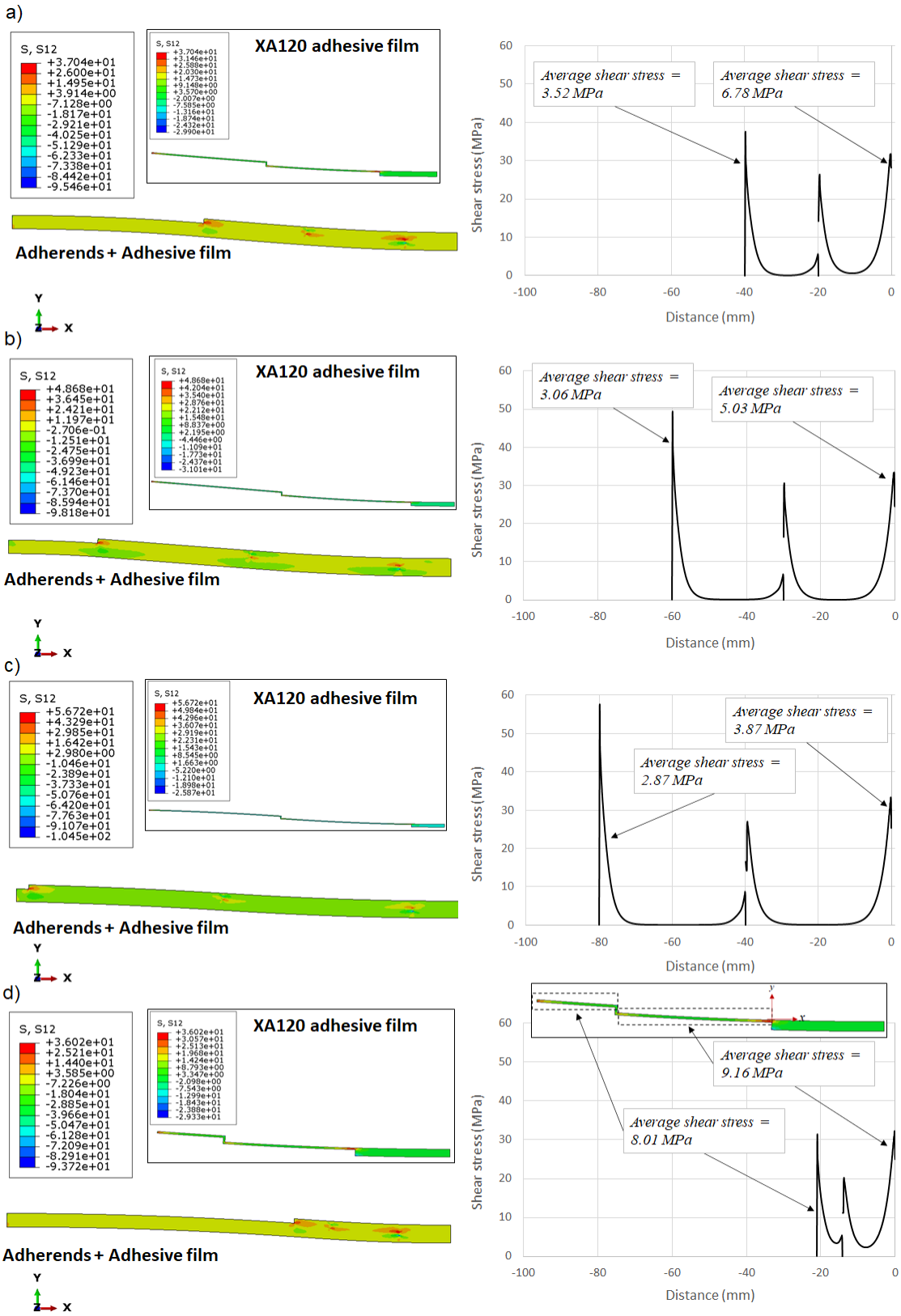

Figure A2: Shear stress (S_{12}) contour plots (left) and shear stress distribution at mid-plane of adhesive (right) for 2D plane strain model of various repair designs at $0.63\ mm$ enforced end displacement, a) repair design A, b) repair design B, c) repair design C and d) repair design D (VLSS). (All units are in MPa)

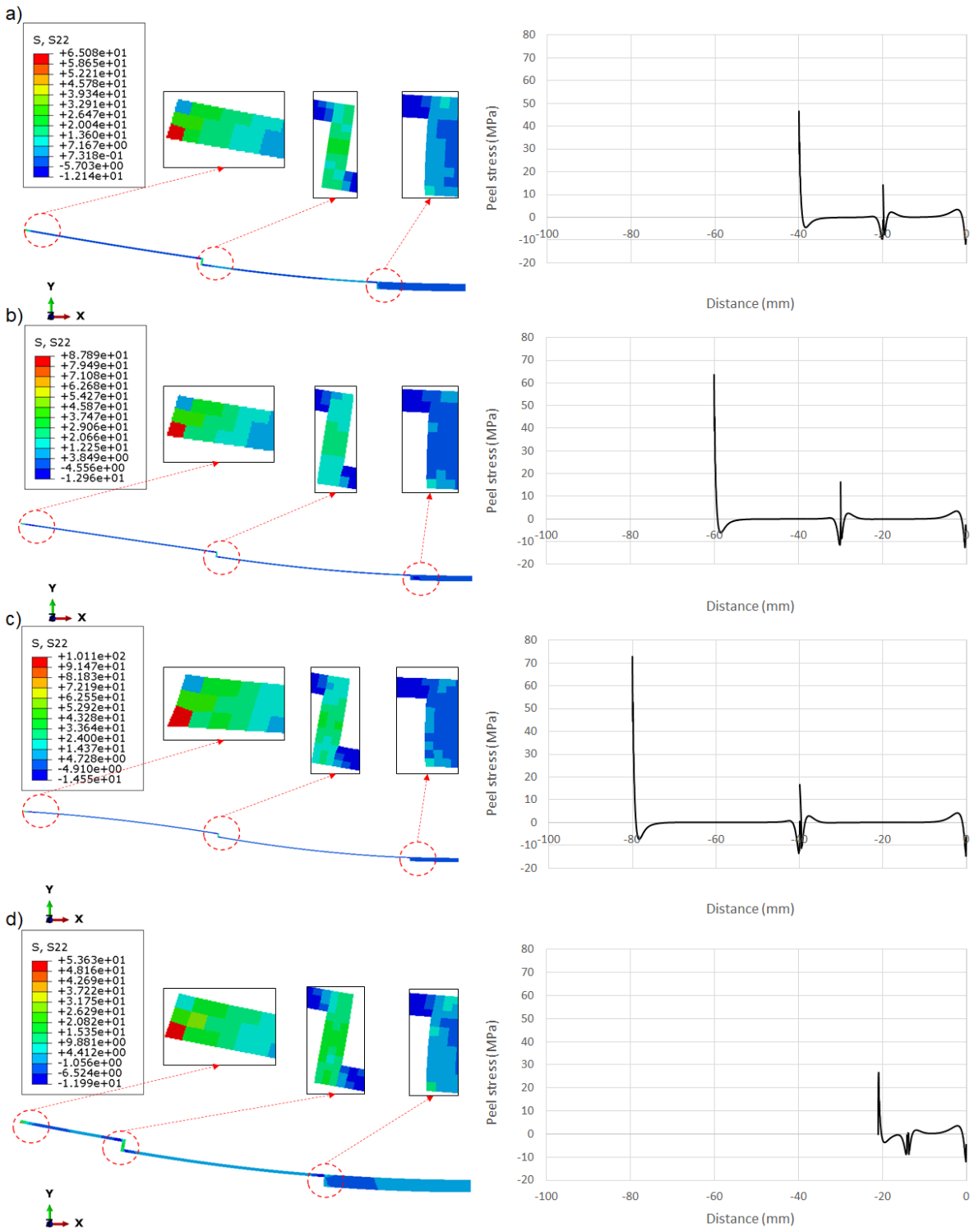

Figure A3: Peel stress (S_{22}) contour plots (left) and peel stress distribution at mid-plane of adhesive (right) for 2D plane strain model of various repair designs at $0.63\ mm$ enforced end displacement, a) repair design A, b) repair design B, c) repair design C and d) repair design D (VLSS). (All units are in MPa)

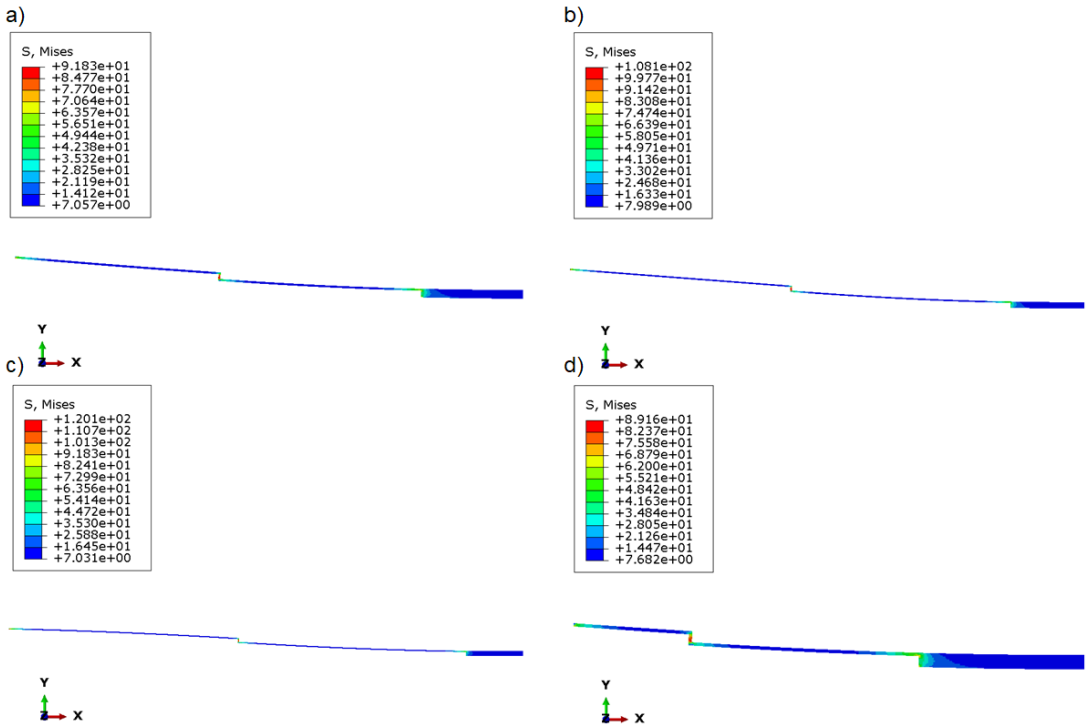

Figure A4: von Mises contour plots within adhesive for 2D plane strain model of various repair designs at $0.63\ mm$ enforced end displacement, a) repair design A, b) repair design B, c) repair design C and d) repair design D (VLSS). (All units are in MPa)

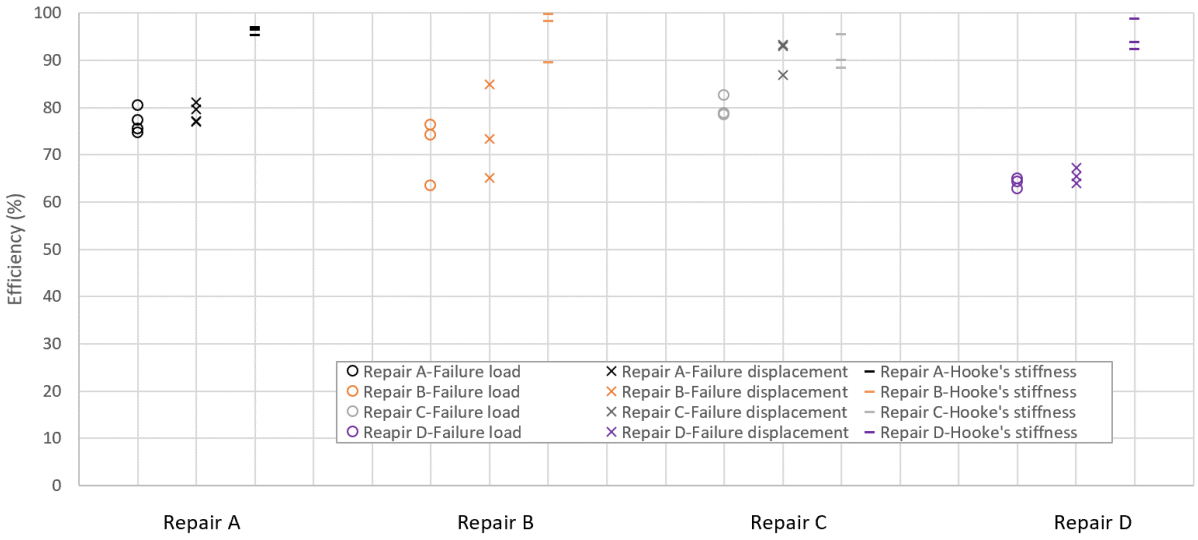

Figure A5: Efficiency scattered data of repair tests

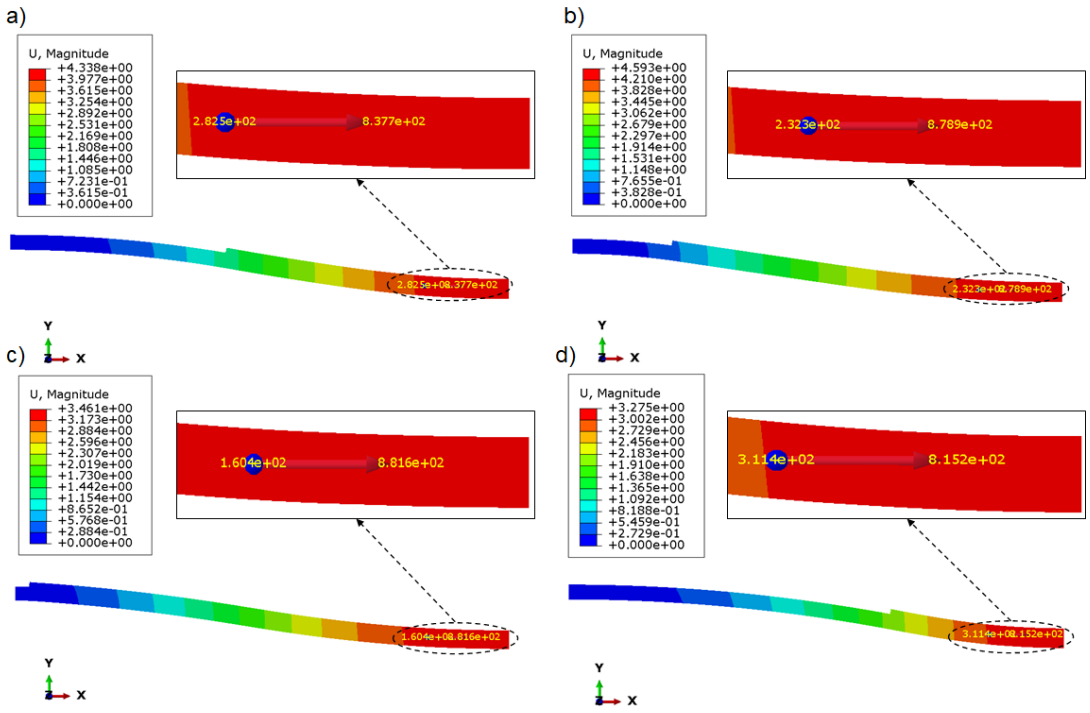

Figure A6: Displacement contour plots and section forces/moments at $0.63\ mm$ enforced end displacement, a) repair design A, b) repair design B, c) repair design C and d) repair design D. (Displacements are in mm, section forces and moments are in N and $N.mm$ per unit of width, respectively)

References

[1] V. Giurgiutiu, "Introduction," in *Structural Health Monitoring of Aerospace Composites*, Elsevier, 2016, pp. 1–23.

[2] M. Suresh Kumar, M. Ambresha, K. Panbarasu, I. Kishore, and V. R. Ranganath, "A comparative study of failure features in aerospace grade unidirectional and bidirectional woven CFRP composite laminates under four-point bend fatigue loads," *Materwiss. Werksttech.*, vol. 46, no. 6, pp. 644–651, 2015, doi: 10.1002/mawe.201400278.

[3] M. H. Kabir, S. Fawzia, T. H. T. Chan, and M. Badawi, "Durability of CFRP strengthened steel circular hollow section member exposed to sea water," *Constr. Build. Mater.*, vol. 118, pp. 216–225, 2016, doi: 10.1016/j.conbuildmat.2016.04.087.

[4] L. Rufail, J. J. Laurin, and F. Moupfouma, "Composite aircraft lightning strike protection damage evaluation using microwave microscopy techniques," 2017, doi: 10.23919/EuCAP.2017.7928331.

[5] C. H. Wang and C. N. Duong, *Bonded Joints and Repairs to Composite Airframe Structures*. Elsevier, 2016.

[6] K. B. Katnam, L. F. M. Da Silva, and T. M. Young, "Bonded repair of composite aircraft structures: A review of scientific challenges and opportunities," *Progress in Aerospace Sciences*, vol. 61. pp. 26–42, 2013, doi:

10.1016/j.paerosci.2013.03.003.

[7] M. Damghani, J. Bakunowicz, and A. Murphy, “Understanding the influence of laminate stacking sequence on strain/stress concentrations in thin laminates at repair holes with large scarf angles,” *J. Compos. Mater.*, vol. 53, no. 28–30, pp. 4273–4284, Jun. 2019, doi: 10.1177/0021998319855772.

[8] B. Liu, F. Xu, W. Feng, R. Yan, and W. Xie, “Experiment and design methods of composite scarf repair for primary-load bearing structures,” *Compos. Part A Appl. Sci. Manuf.*, vol. 88, pp. 27–38, 2016, doi: 10.1016/j.compositesa.2016.05.011.

[9] B. Liu, F. Xu, R. Yan, Z. Ji, and W. Li, “Parameters sensitivity and optimization for composite scarf repair,” *J. Reinf. Plast. Compos.*, vol. 33, no. 23, pp. 2164–2173, 2014, doi: 10.1177/0731684414555744.

[10] T. D. Breitzman, E. V. Iarve, B. M. Cook, G. A. Schoeppner, and R. P. Lipton, “Optimization of a composite scarf repair patch under tensile loading,” *Compos. Part A Appl. Sci. Manuf.*, vol. 40, no. 12, pp. 1921–1930, 2009, doi: 10.1016/j.compositesa.2009.04.033.

[11] C. Wu, C. Chen, L. He, and W. Yan, “Comparison on damage tolerance of scarf and stepped-lap bonded composite joints under quasi-static loading,” *Compos. Part B Eng.*, vol. 155, pp. 19–30, 2018, doi: https://doi.org/10.1016/j.compositesb.2018.08.031.

[12] L. Liao, T. Sawa, and C. Huang, “Numerical analysis on load-bearing capacity and damage of double scarf adhesive joints subjected to combined loadings of tension and bending,” *Int. J. Adhes. Adhes.*, vol. 53, pp. 65–71, 2014, doi: 10.1016/j.ijadhadh.2014.01.010.

[13] E. Ghazali, M. L. Dano, A. Gakwaya, and C. O. Amyot, “Mechanical performance of repaired sandwich panels: Experimental characterization and finite-element modelling,” *J. Sandw. Struct. Mater.*, vol. 21, no. 4, pp. 1357–1378, 2019, doi: 10.1177/1099636217716059.

[14] Q. Han, B. Liu, and W. Xie, “The tension failure mechanisms of composite stepped bonding repairs and joints for the aircraft primary load-bearing structures,” *J. Adhes. Sci. Technol.*, vol. 33, no. 7, pp. 675–690, Apr. 2019, doi: 10.1080/01694243.2018.1558477.

[15] C. H. Wang, V. Venugopal, and L. Peng, “Stepped flush repairs for primary composite structures,” *J. Adhes.*, vol. 91, no. 1–2, pp. 95–112, 2015, doi: 10.1080/00218464.2014.896212.

[16] S. Psarras, T. Loutas, G. Galanopoulos, G. Karamadoukis, G. Sotiriadis, and V. Kostopoulos, “Evaluating experimentally and numerically different scarf-repair methodologies of composite structures,” *Int. J. Adhes. Adhes.*, vol. 97, p. 102495, 2020, doi: https://doi.org/10.1016/j.ijadhadh.2019.102495.

[17] H. Bendemra, P. Compston, and P. J. Crothers, “Optimisation study of tapered scarf and stepped-lap joints in composite repair patches,” *Compos. Struct.*, vol.

130, pp. 1–8, 2015, doi: 10.1016/j.compstruct.2015.04.016.

[18] J.-S. Yoo, V.-H. Truong, M.-Y. Park, J.-H. Choi, and J.-H. Kweon, “Parametric study on static and fatigue strength recovery of scarf-patch-repaired composite laminates,” *Compos. Struct.*, vol. 140, pp. 417–432, 2016, doi: 10.1016/j.compstruct.2015.12.041.

[19] E. Ghazali, M.-L. L. Dano, A. Gakwaya, and C.-O. O. Amyot, “Experimental and numerical studies of stepped-scarf circular repairs in composite sandwich panels,” *Int. J. Adhes. Adhes.*, vol. 82, pp. 41–49, 2018, doi: https://doi.org/10.1016/j.ijadhadh.2017.12.008.

[20] P. E. Irving and C. Soutis, *Polymer Composites in the Aerospace Industry*. Elsevier Ltd, 2014.

[21] F. Collombet *et al.*, “Proof of a composite repair concept for aeronautical structures: a simplified method,” *Mech. Ind.*, vol. 20, no. 8, p. 812, 2019, doi: 10.1051/meca/2020056.

[22] S.-H. A. and G. S. Springer, “Repair of Composite Laminates - Importante metodologia,” no. December, pp. 1–85, 2000.

[23] C. H. Wang and A. J. Gunnion, “On the design methodology of scarf repairs to composite laminates,” *Compos. Sci. Technol.*, vol. 68, pp. 35–46, 2008, doi: 10.1016/j.compscitech.2007.05.045.

[24] M. Damghani, C. Wallis, J. Bakunowicz, and A. Murphy, “Using laminate hybridisation (CFRP-GFRP) and shaped CFRP plies to increase plate post-buckling strain to failure under shear loading,” *Thin-Walled Struct.*, vol. 162, p. 107543, 2021, doi: https://doi.org/10.1016/j.tws.2021.107543.

[25] N. G. C. Barbosa, R. D. S. G. Campilho, F. J. G. Silva, and R. D. F. Moreira, “Comparison of diferent adhesively‑bonded joint types for mechanical structures,” *Appl. Adhes. Sci.*, vol. 6, no. 15, 2018, doi: https://doi.org/10.1186/s40563-018-0116-1.

[26] L. J. Hart-Smith, “Adhesive Bonded Scarf and Stepped Lap Joints,” NASA Technical Report CR-112237, 1973.

[27] M. K. Kim, D. J. Elder, C. H. Wang, and S. Feih, “Interaction of laminate damage and adhesive disbonding in composite scarf joints subjected to combined in-plane loading and impact,” *Compos. Struct.*, vol. 94, no. 3, pp. 945–953, Feb. 2012, doi: 10.1016/j.compstruct.2011.10.017.

[28] A. M. G. G. Pinto, R. D. S. G. S. G. Campilho, M. F. S. F. S. F. De Moura, and I. R. Mendes, “Numerical evaluation of three-dimensional scarf repairs in carbon-epoxy structures,” in *International Journal of Adhesion and Adhesives*, 2010, vol. 30, no. 5, pp. 329–337, doi: 10.1016/j.ijadhadh.2009.11.001.

[29] J. Y. Goh, S. Georgiadis, A. C. Orifici, and C. H. Wang, “Effects of bondline flaws on the damage tolerance of composite scarf joints,” *Compos. Part A Appl. Sci. Manuf.*, vol. 55, pp. 110–119, Dec. 2013, doi:

10.1016/j.compositesa.2013.07.017.

[30] M. G. Song *et al.*, “Effect of manufacturing methods on the shear strength of composite single-lap bonded joints,” *Compos. Struct.*, vol. 92, no. 9, pp. 2194–2202, 2010, doi: 10.1016/j.compstruct.2009.08.041.

[31] Y.-M. Jen, “Fatigue life evaluation of adhesively bonded scarf joints,” *Int. J. Fatigue*, vol. 36, no. 1, pp. 30–39, 2012, doi: https://doi.org/10.1016/j.ijfatigue.2011.08.018.

[32] G. A. Atkinson and J. D. Ernst, “High-sensitivity analysis of polarization by surface reflection,” *Mach. Vis. Appl.*, vol. 29, no. 7, pp. 1171–1189, 2018, doi: 10.1007/s00138-018-0962-7.

[33] M. Schoberl, K. Kasnakli, and A. Nowak, “Measuring strand orientation in carbon fiber reinforced plastics (CFRP) with polarization,” *19th World Conf. Non-Destructive Test. (WCNDT 2016)*.

[34] Z. Xie, X. Li, and Q. Yan, “Scarf Repair of Composite Laminates,” *MATEC Web Conf.*, vol. 61, p. 05019, Jun. 2016, doi: 10.1051/matecconf/20166105019.

[35] A. S. M. Al-Azzawi, L. F. Kawashita, and C. A. Featherston, “Buckling and postbuckling behaviour of Glare laminates containing splices and doublers. Part 2: Numerical modelling,” *Compos. Struct.*, vol. 176, pp. 1170–1187, 2017, doi: https://doi.org/10.1016/j.compstruct.2017.04.063.

[36] V.-H. Truong, B.-S. Kwak, R. Roy, and J.-H. Kweon, “Cohesive zone method for failure analysis of scarf patch-repaired composite laminates under bending load,” *Compos. Struct.*, vol. 222, p. 110895, 2019, doi: https://doi.org/10.1016/j.compstruct.2019.110895.

[37] L. F. M. da Silva, A. Ochsner, and R. Adams, *Handbook of Adhesion Technology*. Springer, Cham, 2011.

[38] S. Li, T. Sun, C. Liu, W. Yang, and Q. Tang, “A study of laser surface treatment in bonded repair of composite aircraft structures,” *R. Soc. Open Sci.*, vol. 5, no. 3, p. 171272, Jun. 2021, doi: 10.1098/rsos.171272.

[39] M. Damghani, J. Bakunowicz, and A. Murphy, “Understanding the influence of laminate stacking sequence on strain/stress concentrations in thin laminates at repair holes with large scarf angles,” *J. Compos. Mater.*, vol. 53, no. 28–30, 2019, doi: 10.1177/0021998319855772.

[40] U. A. Khashaba and I. M. R. Najjar, “Adhesive layer analysis for scarf bonded joint in CFRE composites modified with MWCNTs under tensile and fatigue loads,” *Compos. Struct.*, vol. 184, pp. 411–427, Jan. 2018, doi: 10.1016/J.COMPSTRUCT.2017.09.095.

[41] J. Y. Cognard, L. Sohier, and P. Davies, “A modified Arcan test to analyze the behavior of composites and their assemblies under out-of-plane loadings,” *Compos. Part A Appl. Sci. Manuf.*, vol. 42, no. 1, pp. 111–121, Jan. 2011, doi: 10.1016/J.COMPOSITESA.2010.10.012.

Dr. Mahdi Damghani
(CEng MIMechE, PhD, MSc, BSc)
Senior Lecturer in Composites and Aero-structures
Room 3D26
Engineering Design and Mathematics Department
University of the West of England (UWE)
Frenchay Campus
Coldharbour Lane
Bristol
BS16 1QY
Tel: 0117 328 7369
Email: Mahdi.Damghani@uwe.ac.uk

Date: 17/08/2021

Dear Editor,

This letter is to declare no conflict of interest in carrying out the research by the authors titled as “Design, novel quality check and experimental test of an original variable length stepped scarf repair scheme”.

Yours’ Sincerely

Dr Mahdi Damghani
Stephan Bolanos
Amandeep Chahar
Dr Gary A. Atkinson
Dr Jason Matthews
Prof Adrian Murphy
Timothy Edwards

CRediT author statement:

Mahdi Damghani: Conceptualisation, Methodology, Software, Validation, Formal analysis, Resources, Writing-Original Draft, Writing-Review & Editing, Visualisation, Supervision, Project administration **Stephan Bolanos:** Investigation, Data Curation **Amandeep Chahar:** Investigation, Data Curation **Gary Atkinson:** Investigation, Data Curation, Writing-Review & Editing **Jason Matthews:** Data Curation, Writing-Review & Editing **Adrian Murphy:** Writing-Original Draft, Writing-Review & Editing **Timothy Edwards:** Conceptualisation, Writing-Review & Editing